Univerzita Karlova v Praze
Matematicko-fyzikální fakulta

DIPLOMOVÁ PRÁCE

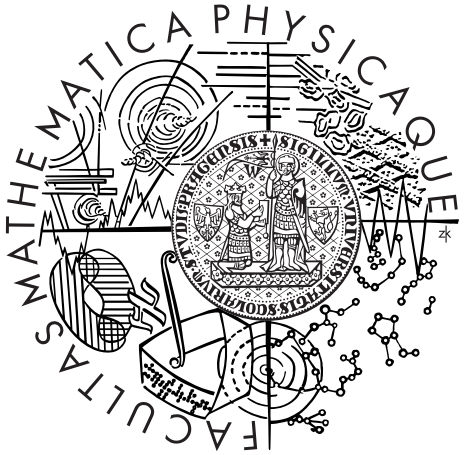

Mgr. Vojtěch Patočka

Predikce pohybů rotační osy řešením Liouvillovy rovnice

Katedra geofyziky

Vedoucí diplomové práce:	doc. RNDr. Ondřej Čadek, CSc.
Studijní program:	Fyzika
Studijní obor:	geofyzika

Praha 2013

Charles University in Prague
Faculty of Mathematics and Physics

MASTER THESIS

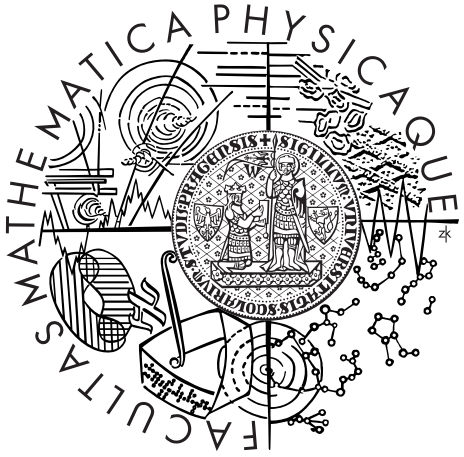

Mgr. Vojtěch Patočka

Polar wander prediction based on the solution of the Liouville equation

Department of Geophysics

Supervisor of the master thesis: doc. RNDr. Ondřej Čadek, CSc.
Study programme: Physics
Specialization: Geophysics

Prague 2013

Mé díky patří všem členům katedry geofyziky. Studovat pod vedením vždy ochotným diskutovat nad dotazy pro mě byla opravdová radost. Zvláště děkuji docentu Čadkovi. Jeho nadhled a vstřícnost mi dodávaly nezbytný klid a přesně cílenými radami mi pomohl zdárně se prokousat problémy s druhou kapitolou. Velký dík patří také profesoru Martincovi, jehož dvoudílný intenzivní kurz mi osvětlil mnohé. Numerickou artilérii s úsměvem předával doktor Hanyk, v letním krizovém štábu zasedala docentka Čížková. Závěrem moc děkuji rodičům, kteří mé lehce prodloužené studium sponzorovali.

I declare that I carried out this master thesis independently, and only with the cited sources, literature and other professional sources.

I understand that my work relates to the rights and obligations under the Act No. 121/2000 Coll., the Copyright Act, as amended, in particular the fact that the Charles University in Prague has the right to conclude a license agreement on the use of this work as a school work pursuant to Section 60 paragraph 1 of the Copyright Act.

In Prague date ..... signature of the author

Název práce: Predikce pohybů rotační osy řešením Liouvillovy rovnice

Autor: Mgr. Vojtěch Patočka

Katedra: Katedra geofyziky

Vedoucí diplomové práce: doc. RNDr. Ondřej Čadek, CSc., katedra geofyziky

Abstrakt: Předmětem práce je hledání numerických řešení Liouvillovy rovnice pro vybrané procesy. Úloha je formulována v Tisserandových souřadnicích a rovnici řešeníme v aproximaci nulového momentu vnějších sil. Žádná další zjednodušení nejsou provedena. V práci je ukázáno, že pro studovaná tělesa má smysl predikovat pohyb rotačního pólu aplikací standardních numerických metod na tuto nezjednodušenou rovnici, a to i pro dlouhodobé procesy. Výsledky jsou porovnány s řešeními, která získáme aplikací aproximativních metod vyvinutých předchozími autory. Na rozdíl od těchto metod volná nutace není odstraněna z Liouvillovy rovnice, a v řešeních tak lze pozorovat její excitaci a útlum. Podmínkou pro řešení úlohy je i studium odezvy tělesa na časově proměnný rotační potenciál. Tato odezva, v podobě rotační deformace, je počítána spektrální konečně-diferenční metodou. Při formulaci příslušných polních rovnic je aplikován Eulerovský přístup. Studujeme pouze tělesa s viskoelastickým pláštěm a tekutým jádrem, v plášti lze předepsat hloubkově závislou hustotu, viskozitu i modul torze. Deformace je počítána přímo v časové oblasti, takže propojení s Liouvillovou rovnicí je přímočaré. První kapitola obsahuje netradiční odvození Liouvillovy rovnice, založené na vyčíslení efektu tzv. nepravých sil v zákonu zachování momentu hybnosti.

Klíčová slova: Pohyb rotační osy, Liouvillova rovnice, viskoelastická relaxace

Title: Polar wander prediction based on the solution of the Liouville equation

Author: Mgr. Vojtěch Patočka

Department: Department of Geophysics

Supervisor: doc. RNDr. Ondřej Čadek, CSc., Department of Geophysics

Abstract: The present thesis seeks numerical solution of the Liouville equation for selected processes. Tisserand's axes are chosen as frame of reference. The only approximation made in the equation is assumtion of zero external torque. It is shown in the present work that it is reasonable to predict the polar wander of the studied models by applying standard numerical methods to this non-simplified equation, and even for long-term processes. The results are compared with solutions gained by approximative methods developed by previous authors. Because free wobble is not filtered out from the Liouville equation, its excitation and damping is observed and may be analyzed. Body's response to centrifugal potential must also be determined in order to treat the Liouville equation properly. This response, i.e. the rotational deformation, is computed using spectral finite-difference method, Eulerian approach is employed to formulate the appropriate set of field equations. Viscoelastic mantle and fluid core are assumed, mantle can have radially dependent density, viscosity and shear modulus. The deformation is computed directly in the time domain, where it is easily coupled with the Liouville equation. In the first chapter, non-traditional derivation of the Liouville equation is developed. It is based on evaluating the effect of fictious forces in the law of balance of angular momentum.

Keywords: Polar wander, Liouville equation, viscoelastic relaxation

Contents

Introduction

The problem of polar wander has a long history and has been studied mostly with respect to the planet Earth (most cited monograph on this subject being the work of Munk and MacDonald, 1960). The Earth has a very stable rotation, with the true polar wander only 0.1° to 0.2° per million years[1] and free wobble causing the geographical poles to wander with radius of only about 10 meters (e.g. Munk and MacDonald, 1960; Novotný, 1998).

For such a body, various approaches may be considered to solve the equations governing the polar motion (the Liouville equations). We can classify them by two criteria. Firstly by what version of the Liouville equations is employed - either the linearized form, or the full, non-linear form. Secondly by the domain in which the equations are solved - either directly in the time domain, or in the Laplace domain.

Munk and MacDonald (1960) introduced the linearized Liouville equations and used Love-number formalism to express inertia tensor components therein appearing. The Liouville equations decouple into two: the so-called polar motion equation, governing the changes in direction of the rotation vector, and the so-called LOD equation, governing the changes in its magnitude (and thus the length of the day). On the right hand side appears the excitation function, which represents various geophysical processes (e.g. winds, tides, melting of an icecap ...etc.) that cause the rotation vector to change. Munk and MacDonald (1960) find it the principal task of the monograph to evaluate the excitation function for certain processes and to find analytical solutions of the Liouville equations for such functions. For zero excitation function, the polar motion equation gives the free wobble (Chandler wobble) - circular motion of the geographical poles with a period of around 430 days (for a rigid Earth it would be only about 305 days, the difference given by elastic response of the Earth to the instaneous position of the

[1]True polar wander is measured from paleomagnetic data as motion of the paleomagnetic reference frame relative to the hot-spot reference frame - e.g. Richards et al., 1997

rotation vector). In more recent work, Martinec and Hagedoorn (2005) showed that for certain processes - namely the postglacial rebound - the wobbling can be removed from the solution of the polar motion equation by averaging over the wobble period.

The Love numbers, used to describe rotational deformation of the Earth, are traditionally computed in the Laplace domain using the normal modes technique (Peltier, 1974; Wu and Peltier, 1982). Thus it is also convenient to seek the solution of the Liouville equations in the Laplace domain. Wu and Peltier (1984) solved the linearized Liouville equations in the Laplace domain, dropping its time derivative terms to give rise to a theoretical discussion not to be clarified untill Vermeersen and Sabadini (1996). This approximation filters the free wobble out of the solution.

The Laplace transform approach provides an insight into the relevant time scales of the problem. Ricard et al. (1993) used this advantage to develop an approximation of the Liouville equations, which is suitable for studies of long-term phenomena. They showed that for very slow processes (with typical time-scales 1-10 Ma) only few viscoelastic relaxation modes do not get completely relaxed within a time step of change of the excitation function. The tidal and loading Love numbers at play can thus be simplified with the use of their fluid limits. For consistency with their approximation (referenced as quasi fluid behaviour - by Lefftz, 1991) terms causing the free wobble are also neglected.

A short summary of the approaches mentioned above, namely the linearized perturbation scheme by Munk and MacDonald (1960) and the method proposed by Ricard et al. (1993) is given in Appendices A and B of this thesis. All of the above mentioned techniques either make use of the linearized Liouville equations (and thus are applicable only to bodies with high rotational stability) or use the viscoelastic Love numbers, which are convenient only for simple models with shperically symmetric viscosity structure. They also filter out the free wobble and thus cannot explain its excitation or damping.

The first task of this thesis is to develop a tool for computing rotational deformation of an incompressible, viscoelastic, planet-sized body directly in the time domain, allowing models with radially dependent density, viscosity and shear modulus to be studied (with the possibility of considering a 3-D viscosity structure in future). The second is to couple this computation with the the non-simplified Liouville equations in order to predict changes in position and magnitude of the rotation vector for chosen processes, even for bodies that do not have strong rotational stability such as the Earth does[2].

Chapter II focuses on the first step of this task. Spectral finite-difference method is used to compute the deformation of a Maxwell viscoelastic body for a prescribed position and magnitude of the rotation vector (i.e. for a given centrifugal potential). The viscoelastic response is computed directly in the time domain (e.g. Hanyk et al., 1996; Tobie et al., 2008). The desired output of this computation is the inertia tensor (to be plugged into the Liouville equations), so we only need to work with spherical harmonics of degree two, because the tensor can be expressed as a combination of degree two coefficients of the gravitational potential expansion using the MacCullagh formula[3]. The code is tested using the isostatic compensation test. Long-term equatorial bulge is computed for three models, including an Earth-like one. All the models used in the thesis have viscoelastic mantle, fluid core and are spherically symmetric before deformation.

Chapter III deals with the non-linear Liouville equations. Basic numerical methods are tested to solve the system of first order ordinary diferential equations. Following integrators are tried: simple explicit Euler method, higher order explicit Runge-Kutta and Bulirsch-Stoer methods, semi-implicit Rosenbrock and Bader-Deuflhard methods. Since no approximation is made in the Liouville equation,

[2]"From geological and paleomagnetic observations, Runcorn (1984) and Shultz (1986) have argued that the Moon and Mars, respectively, have changed their orientation with respect to their axis of rotation. As a matter of fact, for example, some craters ar the Moon's surface, presently located near the pole, have some characteristics of elements placed in the past on the lunar equator" - Lefftz et al., 1991

[3]Plus one additional piece of information is required, e.g. trace of the inertia tensor

the free wobble is present in the solutions, appearing immidiately after a studied process causes the principal axis of inertia to differ from the rotation axis. On the one hand, this method allows to model the excitation and damping of the free wobble. On the other hand, the set of equations become stiff[4] and we are forced to keep the time-step of integration just a small fraction of the free wobble period. This problem remains no matter which numerical method is used, and thus complicates computation of polar wander for complex models for processes with time scales longer than 1 Ma.

One of the driving ideas behind this work is to find out whether current computational capability does not prove the approximative methods redundant. Solution of the non-linear Liouville equations gained by our simple approach, which is to leave the equations as they are, should coincide with approximative solutions for processes that fall within the application limits of the approximative methods. It is shown in Chapter III that this is indeed the case. In addition, excitation and changes of amplitude of the free wobble are present in the solution. Also, the range of applicability of the method is broader than for the approximative methods.

In the first chapter, attention is shortly paid to the traditional derivation of the Liouville equations. Then we develop an alternative derivation. Our approach is based on evaluating the effect of fictious forces[5], when the law of balance of angular momentum is formulated in a non-inertial frame of reference. We hope this derivation brings a new angle to understanding the equations and the various approximations in which they are used. A separate section deals with choice of the frame of reference, and thus also with the relative angular momentum, because the Tisserand axes are chosen (i.e. zero relative angular momentum frame - Munk and MacDonald, 1960).

[4]"stiffness occurs in a problem where there are two or more very different scales of the independent variable on which the dependent variables are changing" - Press et al., 1986

[5]I.e. forces that act in a non-inertial reference frame, also called pseudo forces - e.g. Feynman, 2006

1. Governing equations

1.1 Traditional derivation of the Liouville equations

The standard way to derive the Liouville equations is to write the law of balance of angular momentum in an inertial reference frame and then to transform all time derivatives into a chosen, non-inertial frame of reference, which has rotational motion relative to the inertial reference frame. The procedure is as follows (e.g. Martinec, 2003):

$$\left(\frac{d\vec{H}}{dt}\right)_{inertial} = \vec{L}, \tag{1.1}$$

where $\vec{H}$ is the angular momentum of the body relative to some point and $\vec{L}$ is the moment of external forces relative to that point. Next we use the Resal theorem (e.g. Novotný, 1998) to transform the time derivative into a different reference frame, which is moving relativly to the inertial reference frame, the rotational part of their relative motion being described by $\vec{\omega}$

$$\left(\frac{d\vec{H}}{dt}\right)_{inertial} = \left(\frac{d\vec{H}}{dt}\right)_{non-inertial} + \vec{\omega} \times \vec{H}.$$

Together we get:

$$\left(\frac{d\vec{H}}{dt}\right)_{non-inertial} + \vec{\omega} \times \vec{H} = \vec{L}.$$

Next, the definition of angular momentum is used:

$$\vec{H} = \int \vec{r} \times \left(\frac{d\vec{r}}{dt}\right)_{inertial} \rho \, dv,$$

where ρ stands for density and dv for volume element. The Resal theorem is again applied:

$$\vec{H} = \int \vec{r} \times \left[\left(\frac{d\vec{r}}{dt} \right)_{non-inertial} + (\vec{\omega} \times \vec{r}) \right] \rho \, dv.$$

With help the of definition of the inertia tensor $\mathbf{J} = \int ((\vec{r} \cdot \vec{r})\mathbf{I} - \vec{r} \otimes \vec{r})\rho \, dv$ we get:

$$\vec{H} = \mathbf{J} \cdot \vec{\omega} + \int \vec{r} \times \vec{v} \rho \, dv = \mathbf{J} \cdot \vec{\omega} + \vec{h},$$

where $\vec{h}$, the relative angular momentum is simply the angular momentum measured in the chosen frame of reference. After plugging into (1.1), the Liouville equation is obtained:

$$\frac{d}{dt}(\mathbf{J} \cdot \vec{\omega} + \vec{h}) + \vec{\omega} \times (\mathbf{J} \cdot \vec{\omega} + \vec{h}) = \vec{L}$$

The physical meaning of $\vec{\omega}$[1] is straightforward: The velocity of every point of our chosen reference frame, when measured in the inertial reference frame, can be expressed as $\vec{v_0} + \vec{\omega} \times (\vec{r_p} - \vec{r_0})$ where $\vec{v_0}$ denotes the velocity of the origin of our reference frame, $\vec{r_0}$ the position of its origin and $\vec{r_p}$ the position of the point. The origin of our reference frame is chosen to lie in the center of mass of the studied body.

1.2 Alternative derivation of the Liouville equations

We developed an alternative derivation of the equations, that might provide a somewhat different insight into the problem. The law of balance of angular

[1] $\vec{\omega}$ describes the relative motion of two reference frames and thus is not strictly a vector, for its transformation properties are somewhat anomalous

momentum is again formulated (e.g. Martinec, 2003):

$$\frac{d\vec{h}}{dt} = \frac{d}{dt}\int_{v(t)} \vec{r}\times\vec{v}\,\rho\,dv = \oint_{s(t)} \vec{r}\times\vec{t}_{(\vec{n})}\,da + \int_{v(t)} \vec{r}\times\vec{f}\,\rho\,dv, \tag{1.2}$$

but this time the law is applied directly in the chosen frame of reference (as the law is valid in all frames of reference). In (1.2) $v(t)$ denotes volume of the body, $s(t)$ its surface and $\vec{t}_{(\vec{n})}$ surface traction. In a non-inertial reference frame, however, the so-called fictious forces have to be considered. The body forces appearing in the second term on the right hand side of (1.2) can thus be separated into external (e.g. gravitational force due to an external body), internal (e.g. gravitational force due to the mass of the body itself) and fictious forces: $\vec{f} = \vec{f}_{ext} + \vec{f}_{int} + \vec{f}_{fic}$. After denoting $\oint_{s(t)} \vec{r}\times\vec{t}_{(\vec{n})}\,da + \int_{v(t)} \vec{r}\times\vec{f}_{ext}\rho\,dv = \vec{L}$, as the effect of external body forces and boundary surface traction is clearly the momentum of external forces, we get:

$$\frac{d\vec{h}}{dt} = \vec{L} + \int_{v(t)} \vec{r}\times\vec{f}_{int}\,\rho\,dv + \int_{v(t)} \vec{r}\times\vec{f}_{fic}\,\rho\,dv \tag{1.3}$$

If only central internal forces (e.g. gravitational force) are considered, the term $\int_{v(t)} \vec{r}\times\vec{f}_{int}dv$ is equal to zero (e.g. Havránek, 2002). The complete list of fictious forces is: $-\vec{\omega}\times(\vec{\omega}\times\vec{r}) - 2\vec{\omega}\times\vec{v} - \frac{d\vec{\omega}}{dt}\times\vec{r} - \frac{d\vec{v}_0}{dt} - \vec{\omega}\times\vec{v}_0$, where $\vec{v}_0$ is the velocity of the origin of the non-inertial referential frame relativ to the inertial reference frame (e.g. Novotný, 1998). The last two forces are clearly homogeneous within the body, and thus terms $\int_{v(t)} \vec{r}\times(-\frac{d\vec{v}_0}{dt} - \vec{\omega}\times\vec{v}_0)\rho\,dv$ are equal to zero, if the origin of the non-inertial reference frame lies in the center of mass of the body (which is our case). We therefore have (besides $\vec{L}$) contributions only from the centrifugal, Corriolis and Euler forces on the right hand side of (1.3). To find their role in the derivation, definition of the inertia tensor is recalled:

$$\mathbf{J} = \int \left((\vec{r}\cdot\vec{r})\mathbf{I} - \vec{r}\otimes\vec{r}\right)\rho\,dv$$

and Reynold's transport theorem (e.g. Martinec, 2003) used to find its time derivative:

$$\frac{d\mathbf{J}}{dt} = \int_{v(t)} \left[\frac{D}{Dt} (\vec{r} \cdot \vec{r})\, \mathbf{I} - \vec{r} \otimes \frac{D\vec{r}}{Dt} - \frac{D\vec{r}}{Dt} \otimes \vec{r} \right] \rho \, dv =$$

$$= \int_{v(t)} [2(\vec{r} \cdot \vec{v})\mathbf{I} - \vec{r} \otimes \vec{v} - \vec{v} \otimes \vec{r}] \, \rho \, dv.$$

Motivated by these expressions, we regroup the terms

$$-\int_{v(t)} \vec{r} \times (\vec{\omega} \times (\vec{\omega} \times \vec{r}))\, \rho \, dv - \int_{v(t)} \vec{r} \times (2\vec{\omega} \times \vec{v})\, \rho \, dv - \int_{v(t)} \vec{r} \times (\frac{d\vec{\omega}}{dt} \times \vec{r})\, \rho \, dv$$

as follows[2]:

$$\frac{d\vec{h}}{dt} = \vec{L} - \int_{v(t)} \left[\frac{d\vec{\omega}}{dt} r^2 - \vec{r}(\frac{d\vec{\omega}}{dt} \cdot \vec{r}) \right] \rho \, dv +$$

$$+ \vec{\omega} \times \int_{v(t)} \vec{r}(\vec{\omega} \cdot \vec{r})\, \rho \, dv \; - \int_{v(t)} [\vec{r}(\vec{\omega} \cdot \vec{v}) - \vec{v}(\vec{r} \cdot \vec{\omega})] \; \rho \, dv -$$

$$- \int_{v(t)} [2\vec{\omega}(\vec{r} \cdot \vec{v}) - \vec{r}(\vec{v} \cdot \vec{\omega}) - \vec{v}(\vec{r} \cdot \vec{\omega})] \; \rho \, dv =$$

$$= \vec{L} - \left(\int_{v(t)} \left[r^2 \mathbf{I} - \vec{r} \otimes \vec{r} \right] \; \rho \, dv \right) \cdot \frac{d\vec{\omega}}{dt} +$$

$$+ \vec{\omega} \times \left(\int_{v(t)} \vec{r} \otimes \vec{r}\, \rho \, dv \right) \cdot \vec{\omega} \; - \; \vec{\omega} \times \int \vec{r} \times \vec{v}\, \rho \, dv -$$

$$- \left(\int_{v(t)} [2(\vec{r} \cdot \vec{v})\mathbf{I} - \vec{r} \otimes \vec{v} - \vec{v} \otimes \vec{r}] \; \rho \, dv \right) \cdot \vec{\omega} =$$

$$= \vec{L} - \frac{d}{dt}(\mathbf{J} \cdot \vec{\omega}) - \vec{\omega} \times (\mathbf{J} \cdot \vec{\omega} + \vec{h}).$$

After moving all terms except $\vec{L}$ to the left hand side, the desired Liouville equation is obtained:

$$\frac{d}{dt}(\mathbf{J} \cdot \vec{\omega} + \vec{h}) + \vec{\omega} \times (\mathbf{J} \cdot \vec{\omega} + \vec{h}) = \vec{L}.$$

This derivation might rise certain doubts about the approximation to be made in the next chapter, which is to neglect of the Corriolis and Euler forces in the

[2]Using $\vec{A} \times (\vec{B} \times \vec{C}) = \vec{B}(\vec{A} \cdot \vec{C}) - \vec{C}(\vec{A} \cdot \vec{B})$ and adding $0 = \vec{r}(\vec{\omega} \cdot \vec{v}) - \vec{r}(\vec{\omega} \cdot \vec{v})$

equations of motion (while keeping only the centrifugal force). However, these forces are neglected only in the equations of motion, which are solved only to obtain the inertia tensor components. Further discussion of this approximation follows at the end of the next section.

1.3 The relative angular momentum

The frame of reference has not been chosen yet. The origin of it was placed in the centre of mass of the studied body, but additional information is necessary. In most of the problems in physics, the additional information would be given by prescribing the motion of the reference frame relative to some inertial reference frame. However, in the problem of polar wander the motion of the reference frame is what we seek, and thus a different information must be given.

The necessity to choose a reference frame is obvious. The role of the relative angular momentum $\vec{h}$ and the rotation vector $\vec{\omega}$ in doing so might not be. For example, the full set of equations for a viscous body inserted into an external homogeneous gravity field[3] is valid in all CM (center of mass) frames, and thus can be solved for any prescribed $\vec{\omega}(t)$. The relative angular momentum $\vec{h}(t)$ is then output of the solution. The other possibility is to prescribe $\vec{h}(t)$, $\vec{\omega}(t)$ being output of the solution, which is what we do.

In the thesis the so-called Tisserand axes are chosen, i.e. $\vec{h}(t)$ is set to zero at all times (Munk and MacDonald, 1960). The same choice is made by Ricard et al. (1993) - $\vec{h}$ is not present in the equation (1) therein. Tisserand axes are also chosen by Martinec and Hegedoorn (2005).

Three miscellaneous remarks follow. (i) It can be shown (Martinec, 2003) that if the displacement field $\vec{u}(\vec{r},t)$ is expanded into spherical harmonics, the value of $\vec{h}(t)$ is determined solely by the coefficients of degree one of the expansion,

[3] By "full set" we mean the following equations:
$\nabla \cdot \tau + \rho \vec{f}_{int} - \rho\vec{\omega} \times \vec{\omega} \times \vec{r} - \rho\vec{\omega} \times \vec{v} - \rho\dot{\vec{\omega}} \times \vec{r} = \rho \left(\frac{\partial \vec{v}}{\partial t} + \vec{v} \cdot \nabla \vec{v} \right)$
$\frac{\partial \rho}{\partial t} + \nabla \cdot (\rho \vec{v}) = 0$
$\tau = -p\mathbf{I} + \eta(\nabla \vec{v} + \nabla^T \vec{v})$
$\frac{d}{dt}(\mathbf{J} \cdot \vec{\omega} + \vec{h}) + \vec{\omega} \times (\mathbf{J} \cdot \vec{\omega} + \vec{h}) = \vec{L}$

and not even all of them are needed. Only the toroidal part of the vector field gives non-zero contribution. By explicitely setting these coefficients equal to zero in every time step, we get $\vec{h}(t) = 0$. However, if no terms were neglected in the equations of motion and the equations were coupled with the Liouville equations, with $\vec{h}(t) = 0$ prescribed in the Liouville equations, our resultant displacement field should have toroidal coefficients on degree one equal to zero automatically, of course.

(ii) The alternative derivation of the Liouville equation brings into question the validity of our approximation (to be made in the following chapter), consisting of neglecting the Corriolis and Euler force in the equations of motion. In this thesis we adopt the approach to solve the full Liouville equations and simultaneously to neglect the Coriolis and Euler force in the field equations of motion (which are solved only to get the inertia tensor components), hoping the resultant inertia tensor does not differ substantially from the one we would obtain had we included them. This approach is commonly used in the current literature (e.g. Ricard et al., 1993; Martinec et al., 2005)[4].

(iii) An interesting result is gained if the Liouville equations are re-derived, following the procedure outlined in the previous section, but the Coriolis and Euler forces are omitted. For zero moment of external forces (i.e. $\vec{L} = 0$) the following result is obtained: $\frac{d\vec{h}}{dt} = -\vec{\omega} \times (\mathbf{J} \cdot \vec{\omega})$. Setting $\vec{h}(t) = 0$ in this equation leads to $-\vec{\omega} \times (\mathbf{J} \cdot \vec{\omega}) = 0$. Surprisingly, this equation is also used to predict the polar wander by some authors (e.g. Lefftz, 1991 - this rough approximation being discussed in Ricard et al., 1993. How they reached this approximation is described in Appendix B).

[4]No matter whether the linearized or non-linear Liouville equations are used - both are the full Liouville equations in this context - meaning the equations are derived as if all three fictious forces were present. What are non-full Liouville equations in this context is explained in the third remark.

1.4 Moment of external forces

The tool developed in this thesis is designed for studies of planet-sized bodies, especially planets and moons which are spinning and orbiting some much heavier body. Since the gravitational potential of the orbited body (and possibly other external masses) is not homogeneous, torques of various frequencies influence the studied body. These effects are not in the centre of our attention and are neglected all through setting $\vec{L} = 0$.

Among possible future applications of the developed tool is to determine the position of a certain body relative to the fixed stars (or some planet). If no external torques were present, this would be straightforward to extract from the solution of the polar wander problem. Since the angular momentum to be conserved in the inertial reference frame lies very close the rotation axis, the rotation axis gives us directly the desired position of the studied body (in the first approximation). Short period forced nutations have small amplitudes and do not affect this possibility. However, the long period precession does and would need to be accounted for in such application, if present.

The final form of the Liouville equations to be solved in the thesis is

$$\frac{d}{dt}(\mathbf{J} \cdot \vec{\omega}) + \vec{\omega} \times (\mathbf{J} \cdot \vec{\omega}) = 0. \tag{1.4}$$

2. Rotational deformation

2.1 Governing equations

The response of a Maxwell-type viscoelastic, hydrostatically prestressed body to a disturbing potential is traditionally modeled with the use of various viscoelastic Love numbers (comprehensive summary e.g. by Wu and Peltier, 1982). Love numbers denoted by k describe the relationship between the disturbing potential and gravitational potential of the deformed body. They are usually computed in the Laplace domain using the normal modes technique described by Peltier (1974). Lagrangian approach[1] is traditionally used to formulate the equations of motion.

In this thesis the equations of motion are formulated using the Eulerian approach and they are solved directly in the time domain (to follow e.g. Tobie et al., 2008). This approach is more convenient for complex models and leaves the possibility of involving a 3-D viscosity structure open. We briefly go through all the standard approximations traditionally made (neglected forces and geometrical linearization). The equations of motion read:

$$\nabla \cdot \boldsymbol{\tau} + \vec{f} = \rho(\frac{\partial \vec{v}}{\partial t} + \vec{v} \cdot \nabla \vec{v}).$$

Among the body forces is the gravitational force $\rho\vec{g}$, which can be written as $(\rho_0(r) + \delta\rho(r,\theta,\phi))(\vec{g}_0(r) + \delta\vec{g}(r,\theta,\phi))$, where $\rho_0(r)$ and $\vec{g}_0(r)$ describe the hydrostatically prestressed initial state. The Cauchy stress tensor can be written as $\boldsymbol{\tau} = -p_0\mathbf{I} - \delta p\mathbf{I} + \mathbf{D}$, where p_0 is again the pressure in the initial state and $\mathbf{D}$ stands for the deviatoric part of the stress tensor. Since we work in a non-inertial reference frame, the fictious forces need to be involved. The full set of

[1] On the Eulerian and Lagrangian approach to continuum mechanics see e.g. Martinec, 2003

field equations of motion for the body is:

$$-\nabla p_0 - \nabla\delta p + \nabla\cdot\mathbf{D} + \rho_0\vec{g}_0 + \rho_0\delta\vec{g} + \delta\rho\vec{g}_0 + \delta\rho\delta\vec{g} - \rho\vec{\omega}\times\vec{\omega}\times\vec{r} - \rho\vec{\omega}\times\vec{v} - \\ - \rho\frac{d\vec{\omega}}{dt}\times\vec{r} - \rho\frac{d\vec{v}_0}{dt} - \rho\vec{\omega}\times\vec{v}_0 + \rho\vec{f}_{ext} = \rho\left(\frac{\partial\vec{v}}{\partial t} + \vec{v}\cdot\nabla\vec{v}\right)$$

Terms $-\nabla p_0 + \rho_0\vec{g}_0$ cancel out because such is the condition for the initial hydrostatic equilibrium. Terms $-\frac{d\vec{v}_0}{dt} - \vec{\omega}\times\vec{v}_0$ are equal to the acceleration of the origin of the chosen reference frame, and thus cancel out with $\vec{f}_{ext}$ - gravity caused by an external body (around which our body is orbiting) and which is considered to be homogeneous within the body. Right-hand side $\rho\left(\frac{\partial\vec{v}}{\partial t} + \vec{v}\cdot\nabla\vec{v}\right)$ is omitted because only slow processes are considered, a step standard in geophysics[2]. Forces $-\rho\vec{\omega}\times\vec{v} - \rho\frac{d\vec{\omega}}{dt}\times\vec{r}$ are also assumed to be negligible, the Coriolis force for the same reason as the previous term. The inconsistency that lies behind neglecting these terms is discussed in section 1.3. Within the framework of this thesis, where free wobbling is involved, especially the neglection of the Euler force should be revised in future analysis. Finally, the term $\delta\rho\delta\vec{g}$ is neglected for it is obviously small compared to other terms, e.g. $\delta\rho\vec{g}_0$. After approximations we get:

$$-\nabla\delta p + \nabla\cdot\mathbf{D} + \rho_0\delta\vec{g} + \delta\rho\vec{g}_0 - \rho\vec{\omega}\times\vec{\omega}\times\vec{r} = 0.$$

Our body is assumed to behave like a Maxwell-type viscoelastic mantle and fluid core. For simplicity, we assume the body to be incompressible. In such case, the density anomaly $\delta\rho(\vec{r},t)$ can be evaluated via $\delta\rho(\vec{r},t) := \rho(\vec{r},t) - \rho_0(r) = \rho_0(|\vec{r}-\vec{u}(\vec{r},t)|,t) - \rho_0(r) = -\vec{u}(\vec{r},t)\cdot\nabla\rho_0(r) + O(u^2)$. The $O(u^2)$ terms are neglected in the Taylor series expansion due to geometrical linearization (only small deformations are studied, with deformation gradient small compared to unity).

The centrifugal force can be expressed using the centrifugal potential $\varphi =$

[2]But quite disputable in the context of time scales of processes studied in the thesis - namely the free wobble

$-\frac{1}{2}\rho(\omega^2 r^2 - (\vec{\omega}\cdot\vec{r})^2)$, where $\rho(\vec{r},t)$ can be replaced by $\rho_0(\vec{r})$ due to geometrical linearization, neglecting $-\frac{1}{2}\delta\rho(\omega^2 r^2 - (\vec{\omega}\cdot\vec{r})^2)$, which is small compared to $-\frac{1}{2}\rho_0(\omega^2 r^2 - (\vec{\omega}\cdot\vec{r})^2)$.

Similarily, the potential Φ is introduced to express the self-gravity term $\rho_0\delta\vec{g}$. The potential is defined as the solution to the Poisson equation $\nabla^2\Phi = 4\pi G\delta\rho$. Final form of the equations to be solved is:

$$-\nabla\delta p + \nabla\cdot\mathbf{D} - (\vec{u}\cdot\nabla\rho_0)\vec{g}_0 - \rho_0\nabla\Phi - \rho_0\nabla\varphi = 0.^3$$

In this thesis we restrain to the study of a body with viscoelastic mantle and fluid core. Maxwell-type viscoelasticity is simple to implement and yields both effects of crucial importance in the presented study: the instaneous elastic response as well as the $t\to\infty$ fluid limit. The amplitude of the instaneous response determines the period of the free wobble and the relaxation time necessary to reach the fluid limit is determining factor in the process of readjustment of the long-term equatorial bulge, as shown in the next chapter. The Maxwell viscoelastic rheology for an incompressible body may be written (e.g. Tobie et al., 2008):

$$\mathbf{D} - \mu(\nabla\vec{u} + (\nabla\vec{u})^T) = -\frac{\mu}{\eta}\int_0^t \mathbf{D}dt'.$$

Since the viscosity is on the right hand side of the equation, which is numerically computed from the previous time-step, it is possible to work with lateral variations of viscosity. This reason is the motivation to solve the equations directly in the time domain (e.g. Hanyk et al., 1996). The set of equations to be solved is thus

[3]The equation can be compared to the one traditionally solved (e.g. Wu and Peltier, 1982; Legros and Lefftz, 1993), which is derived using the Lagrangian description of field quantities. Transformed into our notation, the equations read: $-\nabla\delta p+\nabla\cdot\mathbf{D}-(\vec{u}\cdot\nabla\rho_0)\vec{g}_0-\rho_0\nabla\Phi+\nabla(\rho_0\vec{u}\cdot\vec{g}_0)=0$. The centrifugal potential, assumed to be constant, is included in the initial state here. The only difference between the equations is thus the term $\nabla(\rho_0\vec{u}\cdot\vec{g}_0)$. Also formulation of free surface boundary condition is different in Lagrangian formulation: $\boldsymbol{\tau}_{rr} = \boldsymbol{\tau}_{r\theta} = 0$ instead of $\boldsymbol{\tau}\cdot\vec{e}_r = u_r\rho_0\vec{g}_0$. These two differences should cancel out to yield the same results in both formulations.

the following:

$$-\nabla\delta p + \nabla\cdot\mathbf{D} - (\vec{u}\cdot\nabla\rho_0)\vec{g}_0 - \rho_0\nabla\Phi - \rho_0\nabla\varphi = 0 \tag{2.1}$$

$$\nabla\cdot\vec{u} = 0 \tag{2.2}$$

$$\mathbf{D} - \mu(\nabla\vec{u} + (\nabla\vec{u})^T) = -\frac{\mu}{\eta}\int_0^t \mathbf{D}dt' \,. \tag{2.3}$$

The region of space selected to solve these field equations is a perfect spherical shell of outer radius a. Thus we need to account for the effects of surface and core-mantle topographies through boundary conditions. On the outer surface, zero tangential component of traction is prescribed and the radial component is set to equal out the pressure of surface topography:

$$(-\delta p\mathbf{I} + \mathbf{D})\cdot\vec{e}_r = u_r\rho_0\vec{g}_0{}^{45} \tag{2.4}$$

The situation is more complicated on the core-mantle boundary, for the fluid core is assumed to have high density and thus its pressure must be taken into consideration (contrary to the pressure of the outer atmosphere):

$$-(-\delta p\mathbf{I} + \mathbf{D})\cdot\vec{e}_r = +u_r\Delta\rho_{CMB}\vec{g}_0 + p_c\vec{e}_r$$

The sign on the left hand side is different from the one in (2.4) due to the opposite sign of the outer normal to the surface. The pressure p_c is caused by the centrifugal potential as well as by the gravity potential induced by density anomalies. It can be evaluated as $\rho_{core}(\varphi+\Phi)$, because the hydrostatic equilibrium is assumed to hold at all times within the core: $-\nabla p_c = -\rho_{core}\nabla(\varphi+\Phi)$. The boundary

[4]The tangential component of traction is set to zero because $\vec{g}_0||\vec{e}_r$

[5]Our displacement field is the Eulerian description of displacement $\Rightarrow$ $u_r(R_a,\theta,\phi)$ is not exactly the height of surface topography (which is $u_r(r_{surf}(\theta,\phi),\theta,\phi)$). Due to geometrical linearization the difference is neglected.

condition can therefore be written:

$$-\left(-\delta p\mathbf{I}+\mathbf{D}\right)\cdot\vec{e}_r = u_r\Delta\rho_{CMB}\vec{g}_0+\rho_{core}(\varphi+\Phi)\vec{e}_r \tag{2.5}$$

2.2 Spectral finite-difference method

To solve the set of first order partial differential equations (2.1) - (2.5) we expand all the laterally dependent quantities into complex spherical harmonics, spherical vectors and spherical tensors:

$$\Phi=\sum_{j=0}^{\infty}\sum_{m=-j}^{j}\Phi_{jm}(r)Y_{jm}(\theta,\phi),\quad \varphi=\sum_{j=0}^{\infty}\sum_{m=-j}^{j}\varphi_{jm}(r)Y_{jm}(\theta,\phi)$$

$$\vec{u}=\sum_{j=0}^{\infty}\sum_{m=-j}^{j}\sum_{k=|j-1|}^{j+1}u^k_{jm}(r)\vec{Y}^k_{jm}(\theta,\phi)$$

$$\bar{\boldsymbol{\tau}}=\left(-\delta p\mathbf{I}+\mathbf{D}\right)=-\sum_{j=0}^{\infty}\sum_{m=-j}^{j}\delta p_{jm}(r)\mathbf{Y}^{j,0}_{jm}(\theta,\phi)+\sum_{j=0}^{\infty}\sum_{m=-j}^{j}\sum_{k=|j-2|}^{j+2}D^{k,2}_{jm}(r)\mathbf{Y}^{k,2}_{jm}(\theta,\phi)$$

Spherical harmonics used in the expansion are constructed as a product of the orthogonal basis $e^{im\phi}$ and the fully normalized associated Legendre functions $P_{lm}(\cos\theta)$. Spherical vectors are constructed as a generalized product of spherical harmonics Y_{jm} and the cyclic basis $\vec{e}_\nu$. Spherical tensors are constructed as a generalized product of spherical harmonics Y_{jm} and specially prescribed tensor basis $\mathbf{e}_{\nu,\lambda}$. Their full description and properties can be found in Varshalovich et al. (1988).

In Appendix A of Golle et al. (2012) are selected out the relations relevant to the particular set of equations we solve. The choice of the generalized spherical harmonics introduced by Jones (1985) - i.e. the choice of spherical harmonic basis, is motivated by the fact that tensors are decomposed into isotropic, antisymmetric and deviatoric parts (which we already used in the expansion of $\bar{\boldsymbol{\tau}}$, where we omitted the antisymmetric part because $\bar{\boldsymbol{\tau}}$ is symmetric) and vectors are decomposed into spheroidal and toroidal parts.

The equation of motion (2.1) is a vector equation and as such consists of three equations, one for each of the three components, i.e. one for each of the base vectors $\vec{Y}_{jm}^{j-1}, \vec{Y}_{jm}^{j}, \vec{Y}_{jm}^{j+1}$. To get these equations, relations for the divergence of spherical tensors, radial part of spherical vectors and gradient of shperical harmonics must be put into action. The divergence of the stress tensor equals (Golle et al., 2012):

$$\nabla \cdot \bar{\boldsymbol{\tau}} = \sum_{j=0}^{\infty} \sum_{m=-j}^{j} \Bigg\{ \vec{Y}_{jm}^{j-1} \Bigg[\sqrt{\frac{j}{3(2j+1)}} \Big(\frac{d\delta p_{jm}}{dr} + \frac{(j+1)\delta p_{jm}}{r} \Big) +$$

$$+ \sqrt{\frac{j-1}{2j-1}} \Big(\frac{dD_{jm}^{j-2,2}}{dr} - \frac{j-2}{r} D_{jm}^{j-2,2} \Big) - \sqrt{\frac{(j+1)(2j+3)}{6(2j-1)(2j+1)}} \Big(\frac{dD_{jm}^{j,2}}{dr} + \frac{j+1}{r} D_{jm}^{j,2} \Big) \Bigg] +$$

$$+ \vec{Y}_{jm}^{j} \Bigg[- \sqrt{\frac{j-1}{2(2j+1)}} \Big(\frac{dD_{jm}^{j-1,2}}{dr} - \frac{j-1}{r} D_{jm}^{j-1,2} \Big) + \sqrt{\frac{j+2}{2(2j+1)}} \Big(\frac{dD_{jm}^{j+1,2}}{dr} + \frac{j+2}{r} D_{jm}^{j+1,2} \Big) \Bigg] +$$

$$+ \vec{Y}_{jm}^{j+1} \Bigg[- \sqrt{\frac{j+1}{3(2j+1)}} \Big(\frac{d\delta p_{jm}}{dr} - \frac{j\delta p_{jm}}{r} \Big) +$$

$$\sqrt{\frac{j(2j-1)}{6(2j+3)(2j+1)}} \Big(\frac{dD_{jm}^{j,2}}{dr} - \frac{j}{r} D_{jm}^{j,2} \Big) - \sqrt{\frac{j+2}{2j+3}} \Big(\frac{dD_{jm}^{j+2,2}}{dr} + \frac{j+3}{r} D_{jm}^{j+2,2} \Big) \Bigg] \Bigg\}.$$

To evaluate the $-(\vec{u} \cdot \nabla \rho_0)\vec{g}_0 = -u_r(-\frac{d\rho_0}{dr}) g_0 \vec{e}_r$ term, the following relations are needed:

$$(u_r)_{jm} = \sqrt{\frac{j}{2j+1}} u_{jm}^{j-1} - \sqrt{\frac{j+1}{2j+1}} u_{jm}^{j+1}$$

$$Y_{jm}\vec{e}_r = \sqrt{\frac{j}{2j+1}} \vec{Y}_{jm}^{j-1} - \sqrt{\frac{j+1}{2j+1}} \vec{Y}_{jm}^{j+1}.$$

Thus

$$-u_r(-\frac{d\rho_0}{dr}) g_0 \vec{e}_r = \sum_{j=0}^{\infty} \sum_{m=-j}^{j} \Bigg[\left(-\frac{j}{2j+1} u_{jm}^{j-1} + \frac{\sqrt{j(j+1)}}{2j+1} u_{jm}^{j+1} \right) (-\frac{d\rho_0}{dr}) g_0 \vec{Y}_{jm}^{j-1} +$$

$$+ \left(\frac{\sqrt{j(j+1)}}{2j+1} u_{jm}^{j-1} - \frac{j+1}{2j+1} u_{jm}^{j+1} \right) (-\frac{d\rho_0}{dr}) g_0 \vec{Y}_{jm}^{j+1} \Bigg].$$

The terms $-\rho_0 \nabla \Phi - \rho_0 \nabla \varphi$ are moved to the right hand side of the equation (2.1),

because centrifugal potential is known (in this chapter) and the self-gravity term is computed iteratively in the thesis (viz below).

$$\rho_0 \nabla(\Phi+\varphi) = \sum_{j=0}^{\infty}\sum_{m=-j}^{j}\left[\sqrt{\frac{j}{2j+1}}\left(\frac{d(\Phi+\varphi)_{jm}}{dr}+\frac{j+1}{r}(\Phi+\varphi)_{jm}\right)\vec{Y}_{jm}^{j-1}\right.$$
$$\left.-\sqrt{\frac{j+1}{2j+1}}\left(\frac{d(\Phi+\varphi)_{jm}}{dr}-\frac{j}{r}(\Phi+\varphi)_{jm}\right)\vec{Y}_{jm}^{j+1}\right].$$

The incompressibility condition $\nabla\cdot\vec{u}=0$ is a scalar equation:

$$0 = \sum_{j=0}^{\infty}\sum_{m=-j}^{j}\left[\sqrt{\frac{j}{2j+1}}\left(\frac{du_{jm}^{j-1}}{dr}+\frac{j}{r}u_{jm}^{j-1}\right)Y_{jm}\right.$$
$$\left.-\sqrt{\frac{j+1}{2j+1}}\left(\frac{du_{jm}^{j+1}}{dr}+\frac{j+2}{r}u_{jm}^{j+1}\right)Y_{jm}\right].$$

Finally, the left hand side of (2.3) can be written (the tracelessness and symmetry of $\nabla\vec{u}+(\nabla\vec{u})^T$ is used):

$$2\mu\sqrt{5}\sum_{j=0}^{\infty}\sum_{m=-j}^{j}\left\{\left[\sqrt{j-1}\begin{Bmatrix}1 & 1 & 2\\ j & j-2 & j-1\end{Bmatrix}\left(\frac{du_{jm}^{j-1}}{dr}+\frac{j}{r}u_{jm}^{j-1}\right)\right]\mathbf{Y}_{jm}^{j-2,2}-\right.$$
$$-\left[\sqrt{j}\begin{Bmatrix}1 & 1 & 2\\ j & j-1 & j\end{Bmatrix}\left(\frac{du_{jm}^{j}}{dr}+\frac{j+1}{r}u_{jm}^{j}\right)\right]\mathbf{Y}_{jm}^{j-1,2}-$$
$$-\left[\sqrt{j}\begin{Bmatrix}1 & 1 & 2\\ j & j & j-1\end{Bmatrix}\left(\frac{du_{jm}^{j-1}}{dr}-\frac{j-1}{r}u_{jm}^{j-1}\right)\right]\mathbf{Y}_{jm}^{j,2}+$$
$$+\left[\sqrt{j+1}\begin{Bmatrix}1 & 1 & 2\\ j & j & j+1\end{Bmatrix}\left(\frac{du_{jm}^{j+1}}{dr}+\frac{j+2}{r}u_{jm}^{j+1}\right)\right]\mathbf{Y}_{jm}^{j,2}-$$
$$-\left[\sqrt{j+1}\begin{Bmatrix}1 & 1 & 2\\ j & j+1 & j\end{Bmatrix}\left(\frac{du_{jm}^{j}}{dr}-\frac{j}{r}u_{jm}^{j}\right)\right]\mathbf{Y}_{jm}^{j+1,2}-$$
$$\left.-\left[\sqrt{j+2}\begin{Bmatrix}1 & 1 & 2\\ j & j+2 & j+1\end{Bmatrix}\left(\frac{du_{jm}^{j+1}}{dr}-\frac{j+1}{r}u_{jm}^{j+1}\right)\right]\mathbf{Y}_{jm}^{j+2,2}\right\}-$$
$$-\sum_{j=0}^{\infty}\sum_{m=-j}^{j}\sum_{k=|j-2|}^{j+2}D_{jm}^{k,2}\mathbf{Y}_{jm}^{k,2}=0,$$

where the $\{\}$ brackets denote the 6-j Wigner symbols (Varshalovich et al., 1985).

The integral on the right hand side of (2.3) is numerically evaluated from the previous time step, the increment being $\frac{\mu(r)}{\eta(r)}(D^{k,2}_{jm}(r))_n(t_{n+1}-t_n)$. It is refereneced as the memory term. The memory term is what drives the evolution in time. Without it, instaneous elastic response is obtained.

After plugging all of the above relations into the equations (2.1) - (2.3) we get, for each degree j and order m, a linear system of nine first order ordinary diferential equations for the unknown quantities $u^{j-1}_{jm}, u^{j}_{jm}, u^{j+1}_{jm}, \delta p_{jm}, D^{j-2,2}_{jm}, D^{j-1,2}_{jm}, D^{j,2}_{jm}$, $D^{j+1,2}_{jm}, D^{j+2,2}_{jm}$. In fact, most of the steps already taken were motivated by the final goal to obtain a linear set of ordinary differential equations. First of all, orthogonal base was chosen for the expansion of laterally dependent quantities[6]. Next, the orthogonal base was chosen to be the spherical harmonics, which are eigenfunctions of the diferential operators appearing in the equations. Finally, approximations were made so no products nor squares of laterally dependent quantities appear in the equations. The set of ordinary differential equations can be formulated as follows:

$$\frac{1}{r}\mathbf{A}(r,j)\mathbf{x}(r,j,m) + \mathbf{B}(j)\frac{d\mathbf{x}(r,j,m)}{dr} = \mathbf{y}(r,j,m), \tag{2.6}$$

where we divided the rheological equations by $\mu(r)$. Inspection of the matrices gives an important result, which originally motivated the choice of generalized spherical harmonics introduced by Jones (1985): the equations decouple into a set for six unknowns $u^{j-1}_{jm}, u^{j+1}_{jm}, \delta p_{jm}, D^{j-2,2}_{jm}, D^{j,2}_{jm}, D^{j+2,2}_{jm}$ and a separate set for three unknowns $u^{j}_{jm}, D^{j-1,2}_{jm}, D^{j+1,2}_{jm}$. Since there is no toroidal force on the right hand side of (2.1), the latter set is identically zero and will be further disregarded. After omitting the corresponding lines and columns of $\mathbf{A}$ and $\mathbf{B}$ we get the following form of the matrices (W_{j_1,j_2,j_3} denoting the Wigner 6-j symbols[7]):

[6] scalar products of the equations with the base spherical vectors (equation of motion), spherical tensors (rheology) and spherical harmonics (incompressibility condition) are taken to gain a separate set of equations for each j and m. The vector equation of motion being also broken into three equations and the rheology tensor equation being broken into six equations

[7] e.g. $W_{j,j,j+1} = \left\{ \begin{array}{ccc} 1 & 1 & 2 \\ j & j & j+1 \end{array} \right\}$

$$\mathbf{A}(r,j) = \begin{pmatrix} -\frac{j}{2j+1}(-\frac{d\rho_0}{dr})g_0(r) & \frac{\sqrt{j(j+1)}}{2j+1}(-\frac{d\rho_0}{dr})g_0(r) & -\sqrt{\frac{j}{3(2j+1)}}(j+1) & -\sqrt{\frac{j-1}{2j-1}}(j-2) & -\sqrt{\frac{(j+1)(2j+3)}{6(2j-1)(2j+1)}}(j+1) & 0 \\ \frac{\sqrt{j(j+1)}}{2j+1}(-\frac{d\rho_0}{dr})g_0(r) & -\frac{j+1}{2j+1}(-\frac{d\rho_0}{dr})g_0(r) & -\sqrt{\frac{j+1}{3(2j+1)}}j & 0 & -\sqrt{\frac{j(2j-1)}{6(2j+3)(2j+1)}}j & -\sqrt{\frac{j+2}{2j+3}}(j+3) \\ -\sqrt{\frac{j}{2j+1}}(j-1) & -\sqrt{\frac{j+1}{2j+1}}(j+2) & 0 & 0 & 0 & 0 \\ 2\sqrt{5(j-1)}jW_{j,j-2,j-1} & 0 & 0 & \frac{-r}{\mu(r)} & 0 & 0 \\ 2\sqrt{5j}(j-1)W_{j,j,j-1} & 2\sqrt{5(j+1)}(j+2)W_{j,j,j+1} & 0 & 0 & \frac{-r}{\mu(r)} & 0 \\ 0 & 2\sqrt{5(j+2)}(j+1)W_{j,j+2,j+1} & 0 & 0 & 0 & \frac{-r}{\mu(r)} \end{pmatrix}$$

$$\mathbf{B}(j) = \begin{pmatrix} 0 & 0 & -\sqrt{\frac{j}{3(2j+1)}} & \sqrt{\frac{j-1}{2j-1}} & -\sqrt{\frac{(j+1)(2j+3)}{6(2j-1)(2j+1)}} & 0 \\ 0 & 0 & \sqrt{\frac{j+1}{3(2j+1)}} & 0 & \sqrt{\frac{j(2j-1)}{6(2j+3)(2j+1)}} & -\sqrt{\frac{j+2}{2j+3}} \\ \sqrt{\frac{j}{2j+1}} & -\sqrt{\frac{j+1}{2j+1}} & 0 & 0 & 0 & 0 \\ 2\sqrt{5(j-1)}W_{j,j-2,j-1} & 0 & 0 & 0 & 0 & 0 \\ -2\sqrt{5j}W_{j,j,j-1} & 2\sqrt{5(j+1)}W_{j,j,j+1} & 0 & 0 & 0 & 0 \\ 0 & -2\sqrt{5(j+2)}W_{j,j+2,j+1} & 0 & 0 & 0 & 0 \end{pmatrix}$$

The independece of $\mathbf{A}$ and $\mathbf{B}$ on the order number m should be noticed, a result of symmetries of the involved spherical harmonics. The unknowns are organized into the vector $\mathbf{x}(r,j,m) = (u^{j-1}_{jm}, u^{j+1}_{jm}, \delta p_{jm}, D^{j-2}_{jm}, D^{j}_{jm}, D^{j+2}_{jm})$. Right-hand side $\mathbf{y}(r,j,m)$ contains gradient of the centrifugal potential φ and gradient of the gravitational potential Φ (which is the gravitational potential of the deformed body minus the gravitational potential in the initial state) in its first two components. In the last three components the $-\frac{1}{\eta}\int_0^t \mathbf{D}dt'$[8] is present, which is further referenced as the memory term.

While the memory term is straightforward to evaluate from the previous time step, the increment equal to $\frac{\mu(r)}{\eta(r)}(D^{k,2}_{jm}(r))_n(t_{n+1}-t_n)$, the centrifugal and Φ potentials are less trivial to compute. The centrifugal potential $\varphi = -\frac{1}{2}\rho_0(\omega^2 r^2 - (\vec{\omega}\cdot\vec{r})^2)$ was introduced above. Now it is expanded into spherical harmonics. Since the degree two coefficients of the expansion can be found in e.g. Lefftz et al. (1991)[9], we follow a backward procedure, stating the coefficients first:

$$-\varphi_{20} = \frac{1}{3}\sqrt{\frac{\pi}{5}}(\omega_1^2 + \omega_2^2 - 2\omega_3^2)r^2, \quad -\varphi_{21} = \sqrt{\frac{2\pi}{15}}(\omega_1\omega_3 - i\omega_2\omega_3)r^2$$

$$-\varphi_{22} = \sqrt{\frac{\pi}{30}}(\omega_2^2 - \omega_1^2 + 2i\omega_1\omega_2)r^2,$$

where the minus sign comes from the fact that in this thesis the definition of centrifugal acceleration is chosen to be $-\nabla\varphi$, and not $\nabla\varphi$. Since the potential is a real function, the remaining degree two coefficients are gained by using $\varphi_{j-m} =$

[8] the equations are divided by μ

[9] Only for different kind of spherical harmonics. The expansion given in Lefftz et al., 1991, is however not complete, as proven below, for the zero degree contribution is not given in equation (13) on page 24

$(-1)^m\varphi^*_{jm}$. Let us sum up the degree two expansion:

$$-\tilde{\varphi} := -\sum_{m=-2}^{2}\varphi_{2m}Y_{2m} = \frac{1}{3}\sqrt{\frac{\pi}{5}}(\omega_1^2+\omega_2^2-2\omega_3^2)\frac{1}{4}\sqrt{\frac{5}{\pi}}(3\cos^2\theta-1)r^2+$$

$$+2\mathfrak{Re}\left\{\frac{2\pi}{15}(\omega_1\omega_3-i\omega_2\omega_3)\frac{-1}{2}\frac{15}{2\pi}\sin\theta\cos\theta e^{i\phi}\right\}$$

$$+2\mathfrak{Re}\left\{\sqrt{\frac{\pi}{30}}(\omega_2^2-\omega_1^2+2i\omega_1\omega_2)\frac{1}{4}\sqrt{\frac{15}{2\pi}}\sin^2\theta e^{i2\phi}\right\}r^2 =$$

$$=\Big(-\frac{1}{2}\omega_1\omega_2\sin^2\theta\sin 2\phi-\omega_2\omega_3\sin\theta\cos\theta\sin\phi-\omega_1\omega_3\sin\theta\cos\theta\cos\phi$$

$$-\frac{1}{2}\omega_1^2\sin^2\theta\cos^2\phi+\frac{1}{4}\omega_1^2\sin^2\theta-\frac{1}{2}\omega_2^2\sin^2\theta\sin^2\phi+\frac{1}{4}\omega_1^2\sin^2\theta-$$

$$-\frac{1}{2}\omega_3^2\cos^2\theta+\frac{1}{4}\omega_1^2\cos^2\theta+\frac{1}{4}\omega_2^2\cos^2\theta-\frac{1}{12}\omega_1^2-\frac{1}{12}\omega_2^2+\frac{1}{6}\omega_3^2\Big)r^2 =$$

$$=-\frac{1}{2}(\vec{\omega}\cdot\vec{r})^2+(\frac{1}{4}\omega_1^2+\frac{1}{4}\omega_2^2-\frac{1}{12}\omega_1^2-\frac{1}{12}\omega_2^2+\frac{1}{6}\omega_3^2)r^2=\frac{1}{6}\omega^2r^2-\frac{1}{2}(\vec{\omega}\cdot\vec{r})^2$$

To get the negative of the centrifugal potential $-\varphi=\frac{1}{2}\rho_0(\omega^2r^2-(\vec{\omega}\cdot\vec{r})^2)$, additional term - $\frac{1}{3}\omega^2r^2$ - must be added. Since the term is not laterally dependent, it is simply $\sqrt{\pi}\frac{2}{3}\omega^2r^2Y_{00}$ and thus $\varphi_{00}=-\sqrt{\pi}\frac{2}{3}\omega^2r^2$. An interesting coincidence can be observed. As stated above (and shown below), only the degree two coefficients of the gravitational potential and the trace of the inertia tensor are needed for computation of all the six components of the tensor of inertia. Here it is shown that all the components of centrifugal potential have effect on the tensor of inertia. The degree two coefficients causing deformation that produces degree two coefficients of the gravitational potential and the degree zero coefficient affecting the trace of the inertia tensor. However, in our case the studied body is incompressible and thus the radially symmetric, purely radial force $-\nabla(\varphi_{00}Y_{00})$ causes no deformation (i.e. does not change the trace of the inertia tensor of the initial state).

To solve the system of ODEs (2.6) the finite difference scheme proposed by Gerya and Yuen (2003) is implemented. The method is chosen for its stability

properties and it is a variation of the staggered grid technique. The modeled region (i.e. spherical shell) is divided into layers of constant thicknesses and the unknown quantites are separated: $u_{jm}^{j-1}, u_{jm}^{j+1}$ are placed on the middles of the layers and $\delta p_{jm}, D_{jm}^{k,2}$ are placed on the boundaries of the layers. A four layer model is characterized by the following scheme.

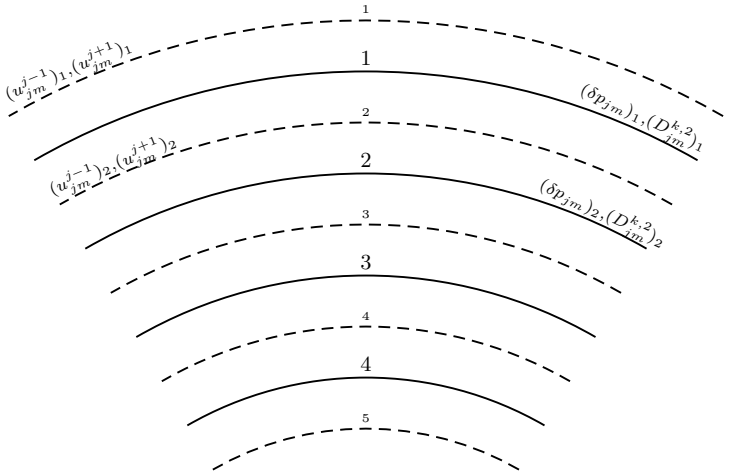

The number of unknowns for an N layered model is $4N$ ($\delta p_{jm}, D_{jm}^{j-2,2}, D_{jm}^{j,2}, D_{jm}^{j+2,2}$ on each boundary) plus $2N+2$ ($u_{jm}^{j-1}, u_{jm}^{j+1}$ on each centre). All the quantities are assumed to be continuous, linear by parts, with jumps of their first derivatives on the boundaries (respectively centres for $u_{jm}^{j-1}(r), u_{jm}^{j+1}(r)$). The equations of motion, which contain the derivatives of $\delta p_{jm}(r), D_{jm}^{k,2}(r)$ are evaluated on the centres of the layers (where $\delta p_{jm}(r), D_{jm}^{k,2}(r)$ are smooth) and the remaining equations, which contain the derivatives of $u_{jm}^{j-1}(r), u_{jm}^{j+1}(r)$ are evaluated on the layer boundaries (where $u_{jm}^{j-1}(r), u_{jm}^{j+1}(r)$ are smooth). The number of equations is thus $6N-2$ ($3N$ rheological equations, N continuity equations, $2(N-1)$ equations of motion), which is 4 less than the number of unknowns. To complete the system of linear equations boundary conditions are necessary. The artificial centres above and below the outer boundaries of the spherical shell

are designed for this purpose. For example, zero displacement boundary condition on the outer surface $\vec{u}(R_a) = 0$ would be implemented simply by putting $(u_{jm}^{j-1})_1 = -(u_{jm}^{j-1})_2, \quad (u_{jm}^{j+1})_1 = -(u_{jm}^{j+1})_2$. Before we implement boundary conditions (2.4) - (2.5), attention si paid to the "self-gravity" term $\rho_0 \nabla\Phi$.

The increment of the gravitational potential caused by deformation of the body can be split into its internal and external parts $\nabla\Phi(r) = \nabla\Phi^e(r) + \nabla\Phi^i(r)$, the external part due to the density anomaly enclosed in the sphere of radius r and the internal part due to the density anomaly outside such sphere. These components can be computed as follows (e.g. Matas, 1995):

$$-\Phi_{jm}^e(r) = \frac{4\pi G r}{2j+1} \int_{R_{CMB}}^{r} \left(\frac{r'}{r}\right)^{j+2} \delta\rho_{jm} dr', \quad r > r' \tag{2.7}$$

$$-\Phi_{jm}^i(r) = \frac{4\pi G r}{2j+1} \int_{r}^{R_a} \left(\frac{r}{r'}\right)^{j-1} \delta\rho_{jm} dr', \quad r' > r \tag{2.8}$$

For a piecewise continuous function $\delta\rho_{jm} = -\vec{u}_{jm} \cdot \nabla\rho_0$ the integrals are computed as follows, r_{c_i} denoting radius of the ith center:

$$-\left(\frac{2j+1}{4\pi G r_{c_i}}\right) \Phi_{jm}^e(r_{c_i}) =$$

$$= \int_{R_{CMB}}^{r_{c_i}} (-\vec{u}_{jm} \cdot \nabla\rho_0) \left(\frac{r'}{r_{c_i}}\right)^{j+2} dr' = \sum_{k=i}^{N} \int_{r_{c_{k+1}}}^{r_{c_k}} (u_r)_{jm} \frac{\rho_{0,k+1} - \rho_{0,k}}{dr} \left(\frac{r'}{r_{c_i}}\right)^{j+2} dr' =$$

$$= \sum_{k=i}^{N} \int_{r_{c_{k+1}}}^{r_{c_k}} \left((u_{r,k})_{jm} + \Delta(u_{r,k})_{jm} \frac{r' - r_{c_k}}{r_{c_{k+1}} - r_{c_k}}\right) \frac{\Delta\rho_{0,k}}{dr} \left(\frac{r'}{r_{c_i}}\right)^{j+2} dr' =$$

$$= \sum_{k=i}^{N} \left[\frac{1}{j+3} \left((u_{r,k})_{jm} + \Delta(u_{r,k})_{jm} \frac{r_{c_k}}{dr_k}\right) \frac{\Delta\rho_{0,k}}{dr_k} \frac{r'^{j+3}}{r_{c_i}^{j+2}} - \frac{\Delta(u_{r,k})_{jm}}{j+4} \frac{\Delta\rho_{0,k}}{dr_k^2} \frac{r'^{j+4}}{r_{c_i}^{j+2}}\right]_{r_{c_{k+1}}}^{r_{c_k}} =$$

$$= \sum_{k=i}^{N} \Bigg[\frac{1}{j+3} \left((u_{r,k})_{jm} + \Delta(u_{r,k})_{jm} \frac{r_{c_k}}{dr_k}\right) \frac{\Delta\rho_{0,k}}{dr_k} \frac{{r_{c_k}}^{j+3} - {r_{c_{k+1}}}^{j+3}}{r_{c_i}^{j+2}} -$$

$$- \frac{\Delta(u_{r,k})_{jm}}{j+4} \frac{\Delta\rho_{0,k}}{dr_k^2} \frac{{r_{c_k}}^{j+4} - {r_{c_{k+1}}}^{j+4}}{r_{c_i}^{j+2}}\Bigg],$$

where notation $\Delta(u_{r,k})_{jm} := (u_{r,k+1})_{jm} - (u_{r,k})_{jm}, \quad \Delta\rho_{0,k} := \rho_{0,k+1} - \rho_{0,k}$ is

introduced. To deal with the lowermost half-layer consistently with the others, $\rho_{0,N+1}$ was set to the density at CMB and $r_{c_{N+1}}$ was put equal to r_{CMB}. Since the thickness of the lowermost half-layer is half the thickness of the other layers, the lower index k next to dr was introduced, meaning $2dr_N = dr, \quad dr_{k\neq N} = dr$. The expression for gravitational potential due to outer mass can be derived analogically. For $j = 2$ we get:

$$-\left(\frac{2j+1}{4\pi G r_{c_i}}\right)\Phi^i_{jm}(r_{c_i}) = \sum_{k=1}^{i-1}\left[\left((u_{r,k})_{jm} + \Delta(u_{r,k})_{jm}\frac{r_{c_k}}{dr_k}\right)\frac{\Delta\rho_{0,k}}{dr_k}\cdot \right.$$
$$\left. \cdot \log\left(\frac{r_{c_k}}{r_{c_{k+1}}}\right) r_{c_i}^{j-1} - \frac{\Delta(u_{r,k})_{jm}}{3-j}\frac{\Delta\rho_{0,k}}{dr_k^2} r_{c_i}^{j-1}(r_{c_k} - r_{c_{k+1}})\right].$$

So far only the density anomalies within a perfect spherical shell were taken into account. Since the studied body has deformed boundaries, the gravitational increment due to the surface topographies must also be evaluated (this contribution being in fact the major one; for a model with homogeneous density it is the only one). Again, we distinguish external part, due to the CMB topography, and in internal part, due to the surface topography[10]

$$-\Phi^{e,topo}_{jm}(r) = \frac{4\pi G r}{2j+1}\Delta\rho_{CMB} t^{CMB}_{jm}\left(\frac{r_{CMB}}{r_{c_i}}\right)^{j+2} \tag{2.9}$$

$$-\Phi^{i,topo}_{jm}(r) = \frac{4\pi G r}{2j+1}\Delta\rho_{surf} t^{surf}_{jm}\left(\frac{r_{c_i}}{r_{surf}}\right)^{j-1}, \tag{2.10}$$

where $\Delta\rho_{CMB}$, $\Delta\rho_{surf}$ denotes the density jumps and t is the height of topographies, which is simply the radial part of the displacement field u_r[11]. To compute this term, the displacement field (i.e. the unknowns) is required. In this thesis the term is thus computed iteratively, the gravitational potential being computed from the displacement field gained in the previous iteration (zero Φ considered in the first step). The advantage of this procedure is that the matrix $\mathbb{A}$ remains

[10] the internal part denoting contribution due to outside mass, the outer surface being always outside for points within the shell

[11] the geometrical linearization is used, viz footnote following the discussion of boundary conditions

band-diagonal (see below). The main disadvantage being the increase of the computational time needed, since it is as many times larger as many iterations are needed. The alternative procedure is to define a new unknown Φ and to include the 'self-gravity' term directly in the matrix $\mathbb{A}$. Since the factorization of $\mathbb{A}$ is to be done only once, this procedure would most likely demand less computational time[12].

Now we have all the expressions needed to transform the set of ODEs (2.6)[13] into a linear problem:

$$\mathbb{A}\,\mathbf{x} = \mathbf{y}. \tag{2.11}$$

To do so, we simply replace all the variables by either their values (e.g. $(u_{jm}^{j-1})_i = u_{jm}^{j-1}(r_{c_i})$) or their averages (e.g. $\frac{1}{2}((u_{jm}^{j-1})_i + (u_{jm}^{j-1})_{i+1})$) - depending on whether their value is demanded on a layer boundary or on a layer center. All the derivatives are replaced with finite differences, e.g. $\frac{(u_{jm}^{j-1})_i - (u_{jm}^{j-1})_{i+1}}{dr_i}$.

The equations of motion, when written on the inner centres of the layered model, give us $2N-2$ rows of the matrix $\mathbb{A}$. The rheological and incompressibility equations are written on all the layer boundaries, providing additional $4N$ rows of $\mathbb{A}$. When all the equations are arranged from surface to CMB, e.g. according their depth, matrix $\mathbb{A}$ becomes band diagonal. So far only $6N-2$ rows were formed, and thus 4 more are needed, because the number of unknowns is $6N+2$. The boundary conditions are the remaining rows, surface BC being the first two rows and CMB boundary conditions being the last two rows of $\mathbb{A}$.

To get the elements of $\mathbb{A}$ due to boundary conditions, following relations are

[12]The reason it is not used in this thesis is purely the simplicity of the iterative approach, making it easier to implement the self-gravity term

[13]where r is the independent variable of the unknows $u_{jm}^{j-1}(r), u_{jm}^{j+1}(r), \delta p_{jm}(r), D_{jm}^{j-2}(r), D_{jm}^{j}(r), D_{jm}^{j+2}(r)$

employed:

$$\bar{\boldsymbol{\tau}} \cdot \vec{e}_r = \sum_{j=0}^{\infty} \sum_{m=-j}^{j} \left\{ \vec{Y}_{jm}^{j-1} \left[\sqrt{\frac{j}{3(2j+1)}} \delta p_{jm} + \sqrt{\frac{j-1}{2j-1}} D_{jm}^{j-2,2} - \sqrt{\frac{(j+1)(2j+3)}{6(2j-1)(2j+1)}} D_{jm}^{j,2} \right] \right.$$
$$\left. + \vec{Y}_{jm}^{j+1} \left[-\sqrt{\frac{j+1}{3(2j+1)}} \delta p_{jm} + \sqrt{\frac{j(2j-1)}{6(2j+3)(2j+1)}} D_{jm}^{j,2} - \sqrt{\frac{j+2}{2j+3}} \right) D_{jm}^{j+2,2} \right] \right\}$$

$$-u_r \rho_0 g_0 \vec{e}_r = \sum_{j=0}^{\infty} \sum_{m=-j}^{j} \left[\left(-\frac{j}{2j+1} u_{jm}^{j-1} + \frac{\sqrt{j(j+1)}}{2j+1} u_{jm}^{j+1} \right) \rho_0 g_0 \vec{Y}_{jm}^{j-1} + \right.$$
$$\left. + \left(\frac{\sqrt{j(j+1)}}{2j+1} u_{jm}^{j-1} - \frac{j+1}{2j+1} u_{jm}^{j+1} \right) \rho_0 g_0 \vec{Y}_{jm}^{j+1} \right].$$

The rotational deformation si computed in order to evaluate components of the tensor of inertia $\mathbf{J}$. The definition of these, when spherical coordinates r, θ, ϕ are used in the integrand, is (e.g. Novotný, 1998):

$$J_{xx} = \int_{v(t)} (\sin^2\theta \sin^2\phi + \cos^2\theta) r^2 \rho dv, \quad J_{yy} = \int_{v(t)} (\sin^2\theta \cos^2\phi + \cos^2\theta) r^2 \rho dv$$

$$J_{zz} = \int_{v(t)} (1 - \cos^2\theta) r^2 \rho dv, \qquad J_{xy} = -\int_{v(t)} \sin^2\theta \cos\phi \sin\phi \, r^2 \rho dv$$

$$J_{xz} = -\int_{v(t)} \sin\theta \cos\phi \cos\phi \, r^2 \rho dv, \qquad J_{yz} = -\int_{v(t)} \sin\theta \cos\phi \sin\phi \, r^2 \rho dv$$

It is integrated over the entire volume, with element dv being $r^2 dr d\Omega$. After decomposing the laterally dependent functions in the integrands into shperical harmonics it is possible to immidiately integrate over $d\Omega$, since ρ can also be expanded into spherical harmonics and the orthogonality properties employed. After following such procedure, equations can be re-written:

$$J_{xx} = \frac{2}{3}\sqrt{\frac{\pi}{5}}\int_{v(t)} r^4\rho_{20}dv + \frac{4}{3}\sqrt{\pi}\int_{v(t)} r^4\rho_{00}dv - \sqrt{\frac{2\pi}{15}}\int_{v(t)} 2\mathfrak{Re}(\rho_{22})r^4dv$$

$$J_{yy} = \frac{2}{3}\sqrt{\frac{\pi}{5}}\int_{v(t)} r^4\rho_{20}dv + \frac{4}{3}\sqrt{\pi}\int_{v(t)} r^4\rho_{00}dv + \sqrt{\frac{2\pi}{15}}\int_{v(t)} 2\mathfrak{Re}(\rho_{22})r^4dv$$

$$J_{zz} = -\frac{4}{3}\sqrt{\frac{\pi}{5}}\int_{v(t)} r^4\rho_{20}dv + \frac{4}{3}\sqrt{\pi}\int_{v(t)} r^4\rho_{00}dv$$

$$J_{xy} = \sqrt{\frac{2\pi}{15}}\int_{v(t)} 2\mathfrak{Im}(\rho_{22})r^4dv, \quad J_{xz} = \sqrt{\frac{2\pi}{15}}\int_{v(t)} 2\mathfrak{Re}(\rho_{21})r^4dv$$

$$J_{yz} = -\sqrt{\frac{2\pi}{15}}\int_{v(t)} 2\mathfrak{Im}(\rho_{21})r^4dv$$

Since $\rho_{2i} = \delta\rho_{2i}$[14], these integrals are closely related to the integrals (2.7) and (2.8). By comparing, the following relationship between tensor of intertia and gravitational potential is obtained (usually referenced as the MacCullagh formulae):

$$\begin{aligned} J_{xx} &= \mathbf{I_0} + \sqrt{\tfrac{\pi}{5}}\tfrac{K}{3}\Phi_{20} - \sqrt{\tfrac{2\pi}{15}}K\Phi_{22}, \quad J_{yy} = \mathbf{I_0} + \sqrt{\tfrac{\pi}{5}}\tfrac{K}{3}\Phi_{20} + \sqrt{\tfrac{2\pi}{15}}K\Phi_{22} \\ J_{zz} &= \mathbf{I_0} - 2\sqrt{\tfrac{\pi}{5}}\tfrac{K}{3}\Phi_{20}, \qquad\qquad J_{xy} = K\sqrt{\tfrac{2\pi}{15}}\mathfrak{Im}(\Phi_{22}) \\ J_{xz} &= K\sqrt{\tfrac{2\pi}{15}}\mathfrak{Re}(\Phi_{21}), \qquad\qquad J_{yz} = -K\sqrt{\tfrac{2\pi}{15}}\mathfrak{Im}(\Phi_{21}) \end{aligned} \tag{2.12}$$

where notation $\mathbf{I_0} := \frac{8}{3}\pi\int_{v(t)} r^4\rho_0 dv$, $K = \frac{5r_{surf}^3}{2\pi G}$ was introduced.

2.3 Computer modelling

To solve the linear problem (2.11) a Fortran code is developed. Its main function is to compose the matrix $\mathbb{A}$. For a model with N layers, $\mathbb{A}$ is an $(6N+2)\times(6N+2)$ band-diagonal matrix. Very efficient solvers have been developed for band-diagonal matrices, here we use the procedure bandec from Numerical Recipes

[14] and $\rho_{00} = \delta\rho_0$

(Press et al., 1992) and procedures from the MKL library. Factorization of $\mathbb{A}$ is done only once, and then solutions for different right-hand sides are sought. Right-hand side $\mathbf{y}$ changes in every time step as the memory term $-\frac{\mu}{\eta}\int_0^t \mathbf{D}dt'$ evolves, the increment needed to get the new value equal to $\frac{\mu(r)}{\eta(r)}(D^{k,2}_{jm}(r))_n(t_{n+1}-t_n)$.

To test the code it is convenient to check the isostatic compensation limit. As described in Wu and Peltier(1982), the response of viscoelastic body to surface loading is as follows: First, elastic response is observed, induced topography only partially supporting the load, stress being induced within the body. In the $t \to \infty$ limit, the induced topography fully compensates the load, stress being again zero within the body.

The load chosen here is an artificial topography, composed of material with density equal to the surface density of the studied model. Load is implemented through the boundary condition (2.4), which is modified:

$$(-\delta p\mathbf{I}+\mathbf{D})\cdot\vec{e}_r = u_r\rho_0\vec{g}_0 + t^{load}\rho_0\vec{g}_0$$

The value of $(t^{load})_{20}$ was set to an arbitrary value of 1253 meters. First, homogeneous model was tested. Parameters of the model are chosen as follows: density set equal to 4000 kg/m^3, shear modulus set to 7×10^{10} Pa and viscosity has the value 1×10^{21} Pa s. This model is further referenced as model A, number of layers is 40. Resulting $(u_r)_{20}$ and component of stress $D^{2,2}_{20}$ are shown in figures 2.1 and 2.2[15]. Displacements of the outer surface, middle layer and CMB boundary are shown. The deformation is driven only by the surface loading, zero centrifugal potential is assumed in the test. Contribution of artificial topography to $\Phi^{i,topo}_{jm}$ is taken into account through replacing t^{surf}_{jm} by $t^{surf}_{jm}+t^{load}_{jm}$ in (2.9). Load is applied at time $t=0$.

All considered models have fluid inner core. The only parameters of the core relevant to our study are its total mass (for computing gravity), moment of inertia

[15]Similar results (regarding the features described below) are gained no matter what degree and order of spherical harmonics is taken

and density at the surface of the core (in order to determine the density jump at CMB). These parameters are set to 1.4490353×10^{23} kg, 8.1888636×10^{36} kg m^2 and 10029 kg/m^3 respectively. These values are derived from the PREM model (Dziewonsky and Anderson, 1981) and are used in all the studied models throughout the thesis.

Figure 2.1: Evolution of $(u_r)_{20}$ for model A

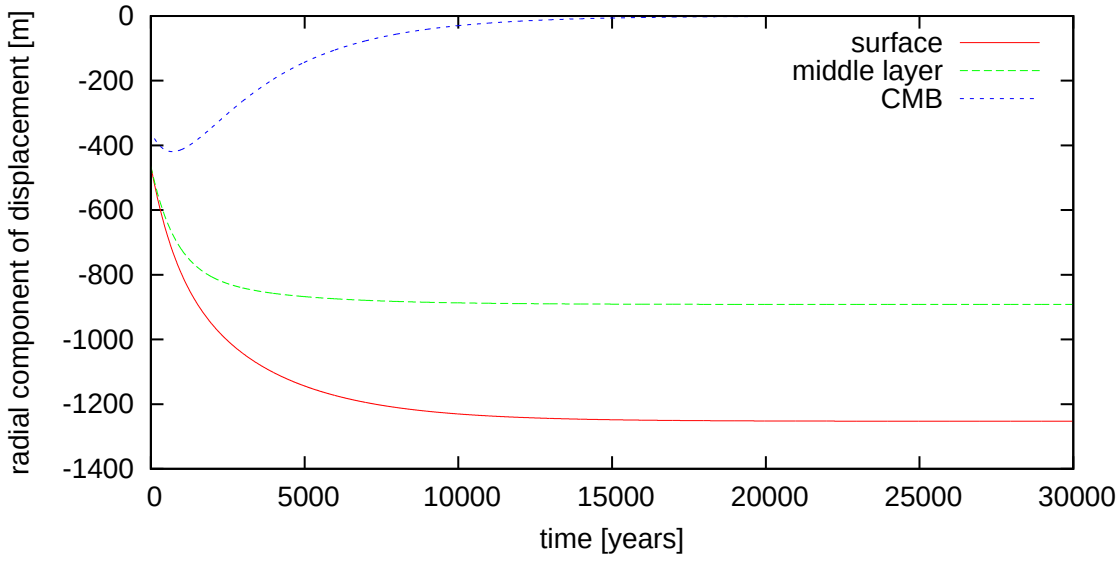

Figure 2.2: Evolution of $(D^{2,2})_{20}$ for model A

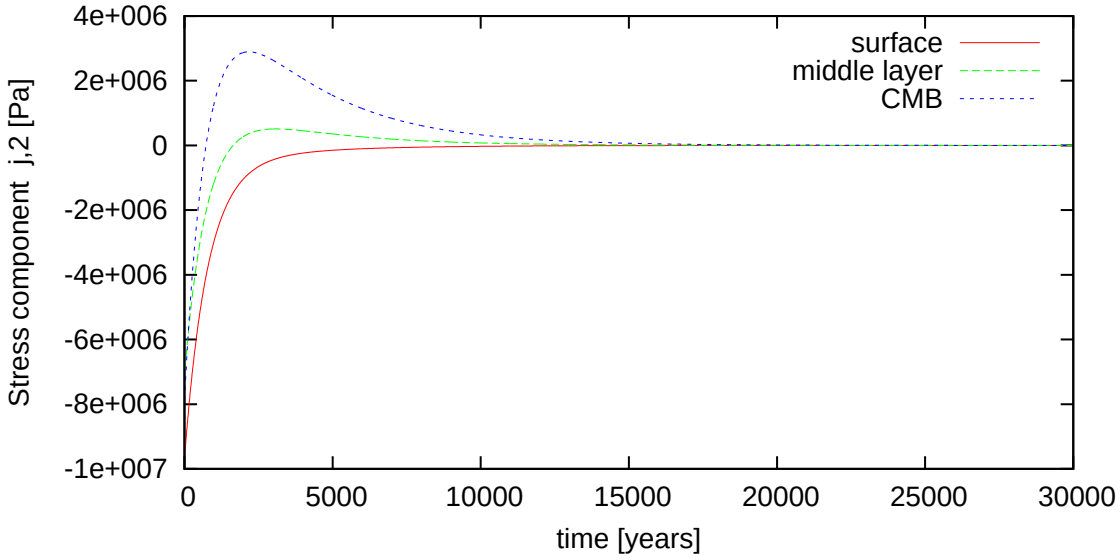

The model responds in the desired way: induced topography is exactly -1253m in the $t \to \infty$ limit and all the components of stress go to zero within the en-

tire body[16]. For a homogeneous model, the $-(\vec{u}\cdot\nabla\rho_0)\vec{g}_0$ term in the equation of motion is identically zero within the body and thus non-zero displacement throughout the mantle is observed even in the $t\to\infty$ limit. Only the inner boundary (CMB) restores its initial zero deformation state, for both δp and $\mathbf{D}$ go to zero, and thus the boundary condition $-(-\delta p\mathbf{I}+\mathbf{D})\cdot\vec{e}_r = +u_r\rho_0\vec{g}_0+\rho_{core}\Phi\vec{e}_r$ demands u_r^{CMB} go to zero, as Φ also goes to zero when u_r^{surf} goes to -1253m.

Qualitatively different response is observed when the model does not have homogeneous density and thus $-(\vec{u}\cdot\nabla\rho_0)\vec{g}_0$ is a non-zero force in the equation of motion. In a model with density increasing with depth, this force acts against the deformation of inner layers[17]. The viscous limit of such model is thus different from the previous one, deformation being concentrated only in the neighbourhood of the body's surface. Response of an inhomogeneous model to loading $(t^{load})_{20} = 1253$ m is shown in figures 2.3 and 2.4. The model's density linearly increases from its surface value 4000 kg/m^3 to 8000 kg/m^3 at the CMB. Remaining parameters are the same as for the homogeneous model, i.e. $\mu = 7\times10^{10}$ Pa and $\eta = 1\times10^{21}$ Pa s. This 40-layer model is further referenced as model B.

Important difference between the response of a homogeneous model and the response of a model with density gradient is in the time needed for the body to relax. Although only models with continuous density profiles are considered (and thus no relaxation normal modes are excited due to inner density discontinuities), the loading Love numbers corresponding to both models have very different evolution in time. While less than 30 thousand years is sufficiently long for the homogeneous model to reach a state with almost perfect relaxation (deviatoric components of the stress tensor being less than 1 Pa, surface displacement being

[16]figure 2.2 shows only the $D^{2,2}$ component. The remaining components, including δp, also have zero limit as $t\to\infty$

[17]this property is of major importance when deformation due to centrifugal potential is studied, for it prohibits the displacement field within the body from diverging. Without this term, centrifugal force causes the inner layers of the body to deform many times more then the outer boundaries → omitting this term in the equation of motion for such model leads to completely wrong results.

Figure 2.3: Evolution of $(u_r)_{20}$ for model B

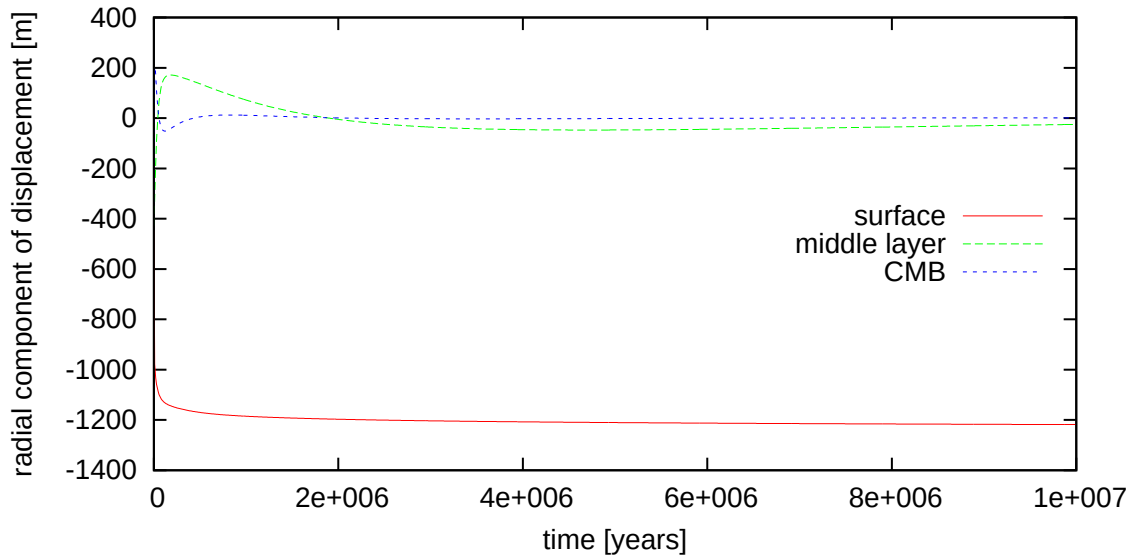

Figure 2.4: Evolution of $(D^{2,2})_{20}$ for model B

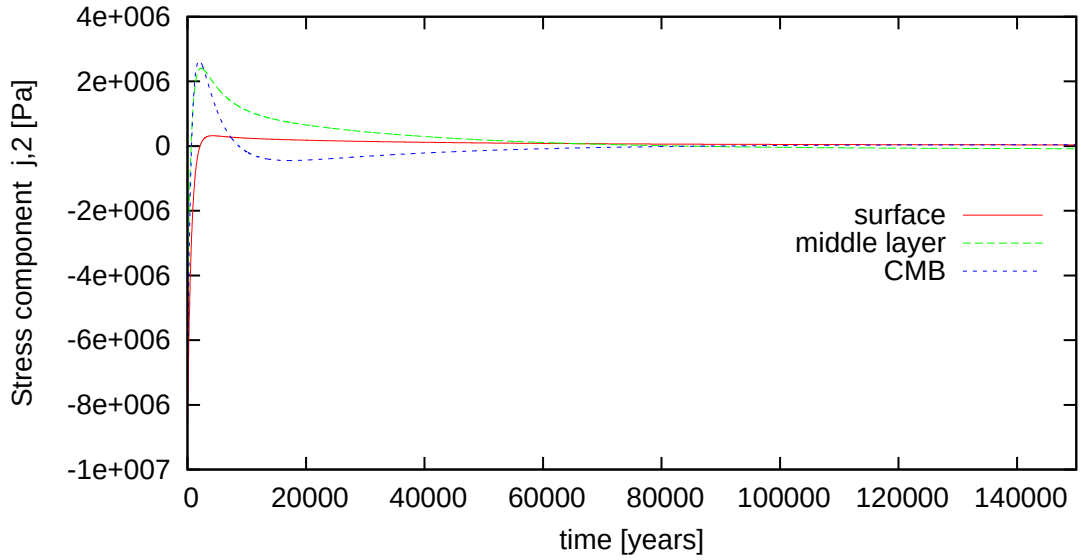

-1253 m with precission to micrometers), more than 10^7 years is needed for the inhomogeneous model to reach the isostatic limit, significant deformation still taking place after 300 thousand years.

Finally, a complex model with chosen density, viscosity and shear modulus profiles is submitted to the isostatic compensation test. Model characteristics are depicted in figure 2.5, model is further referenced as model C. The number

of layers is again 40. It is an Earth-like model, parameters taken from PREM, viscosity chosen arbitrarily. However, a simplification is made: the model's density profile is chosen to be continuous. Dicontinuities, present in the real Earth's mantle due to phase transitions, would have to be dealt with in a similar way boundary conditions deal with density jumps at the boundaries. However, this is not done in the thesis and only continuous profiles are considered. Results of the isostatic test for this model are shown in figure 2.6.

Figure 2.5: Parameters of model C

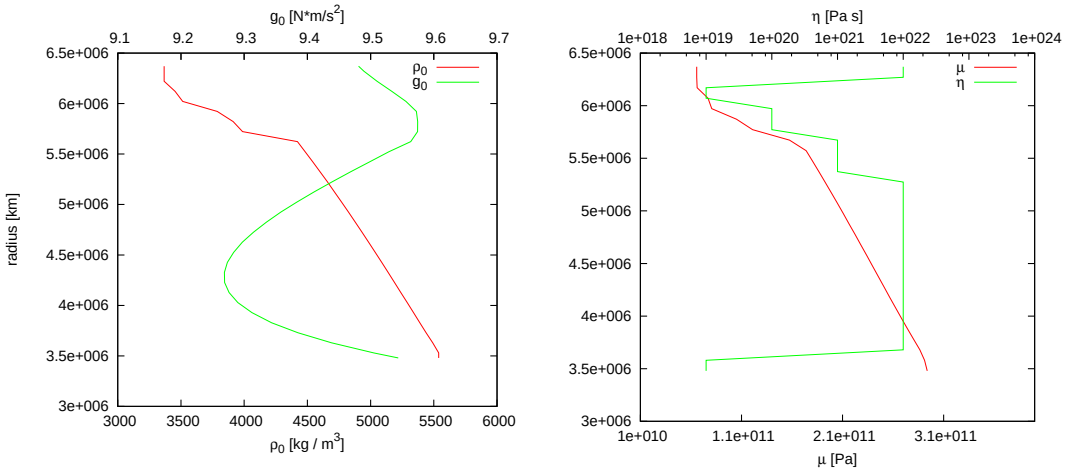

Figure 2.6: Evolution of $(u_r)_{20}$ for model C

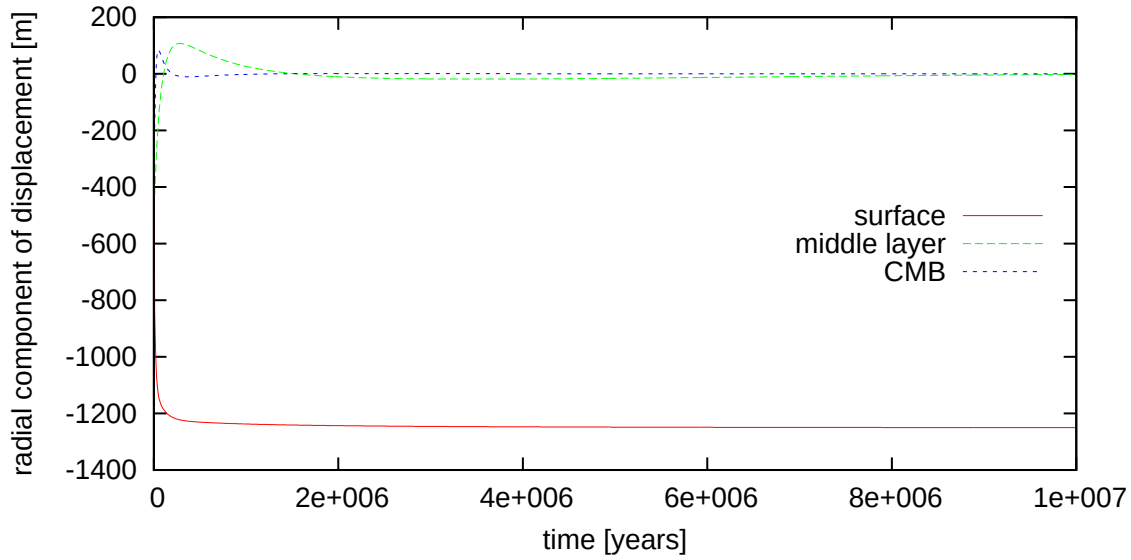

Figure 2.7: Evolution of $(D^{2,2})_{20}$ for model C

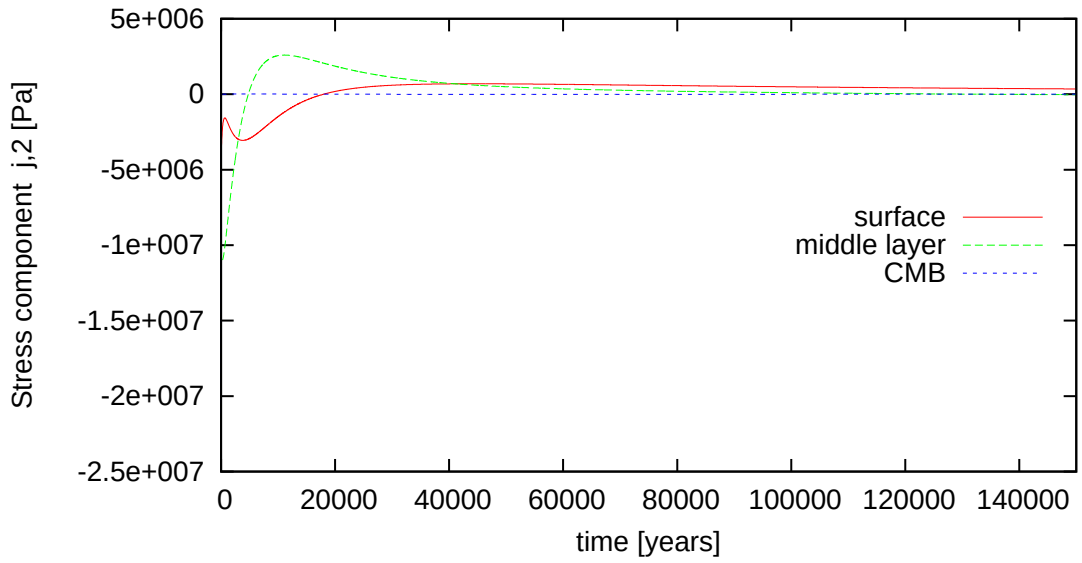

Once the code is tested to give proper response of various models to surface loading, the response to centrifugal potential may be computed. At time $t = 0$ the body is suddenly assumed to rotate with angular velocity $\vec{\omega} = (0, 0, \frac{2\pi}{86400})$ rad s^{-1}, i.e. approximatly the Earth's angular velocity, and appropriate centrifugal force is put into action. Radial components of the resulting displacement fields for models A,B,C are shown in figures 2.8 to 2.10.

Figure 2.8: Evolution of $(u_r)_{20}$ for model A

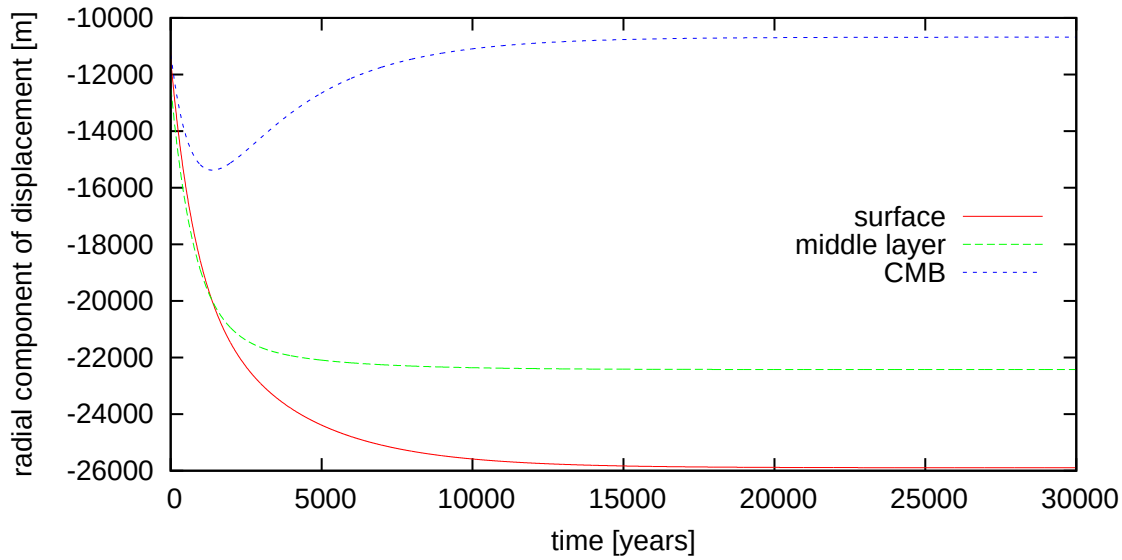

Two basic tests may again be performed to check the corectness of the results.

Figure 2.9: Evolution of $(u_r)_{20}$ for model B

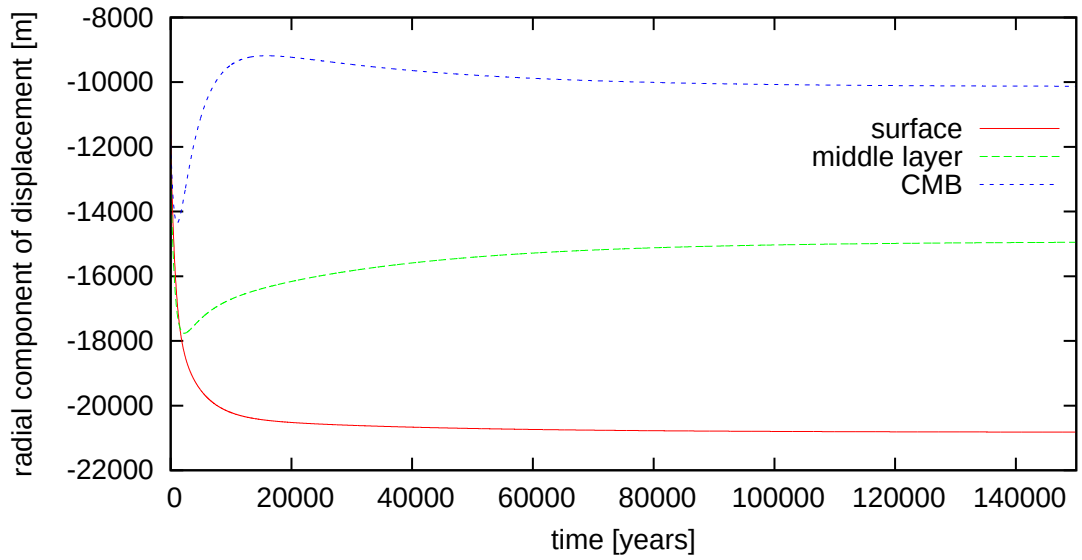

Figure 2.10: Evolution of $(u_r)_{20}$ for model C

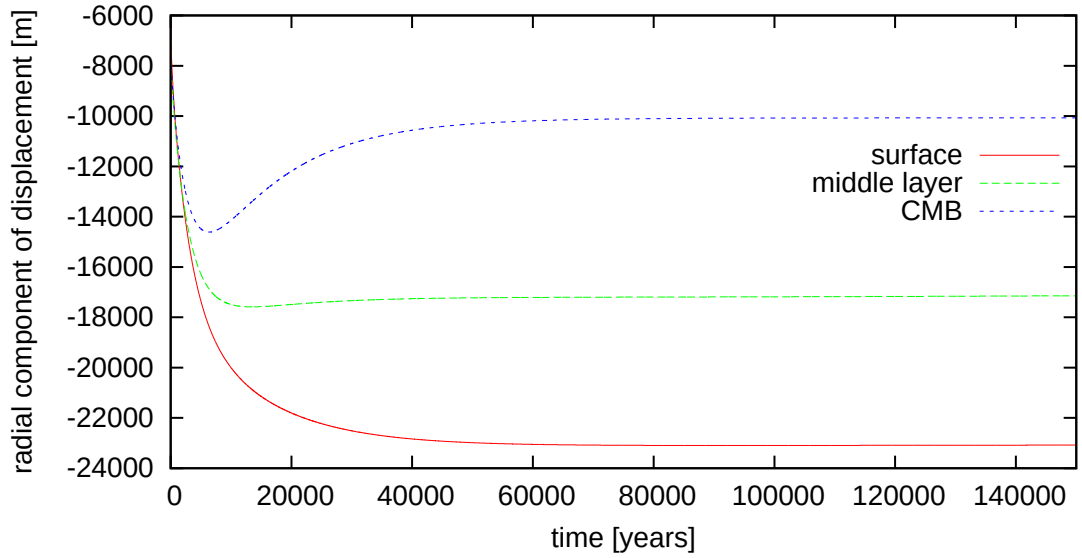

First is that the deviatoric part of the stress tensor goes to zero in the $t \to \infty$, i.e. viscous limit. Second concerns the shape of the deformed body, which must be identical with an equipotential of the disturbing potential in the $t \to \infty$ limit for the state to be stationary. The disturbing potential is the sum of Φ and φ. The height of the equipotential above the surface of the referential sphere can be expressed using the Taylor series expansion of the overall gravity potential, and

replacing its exact gradient with g_0[18]. The condition to be satisfied can thus be written[19]

$$\Phi_{2m} + \varphi_{2m} = (u_r)_{2m} g_0. \tag{2.13}$$

Both tests are satisfied only with limited accuracy by the gained results, the equation (2.13) being satisfied to the precission of meters in the $t \to \infty$ limit and the deviatoric part of the stress tenzor remaining above $10^4 Pa$. However, the accuracy increases as the number of layers of the model is increased[20], which implies it can be explained as error due to discretization in r.

[18] i.e. adopting the Brun theorem

[19] It can be viewed also directly from the governing equations 2.1 and 2.4. If we consider the uppermost layer to be homogeneous, and the deviatoric part of the stress tensor to be zero in the stationary state, equation 2.1 reads $\nabla(\delta p + \rho_0\Phi + \rho_0\varphi) = 0$. Therefore $\delta p + \rho_0\Phi + \rho_0\varphi$ is constant in the uppermost layer. For the degree two coefficients the equation reads $\delta p_{2m} + \rho_0\Phi_{2m} + \rho_0\varphi_{2m} = 0$. Boundary condition on the hand reads $\delta p_{2m} = (u_r)_{2m} * g_0$. After eliminating δp_{2m} from these two equations we get the discussed condition

[20] approximately by factor of 10 when the number of layers is doubled from 40 to 80

3. Polar wander

So far the studied process was relaxation of the body when subjected to a disturbing potential. For centrifugal potential with $\vec{\omega} = (0, 0, \omega_3)$, as was the case in chapter two[1], the resulting tensor of inertia has main axis with the largest moment of inertia parallel to the x_3 axis, i.e. parallel to $\vec{\omega}$. The two remaining main axes lie perpendicular to $\vec{\omega}$. In such case, the $-\vec{\omega} \times (\mathbf{J} \cdot \vec{\omega})$ term is zero in the Liouville equation (1.4). The evolution of $\vec{\omega}(t)$ is then determined solely by the $\frac{d}{dt}(\mathbf{J} \cdot \vec{\omega})$ term, i.e. only ω_3 changes, as the main moment of inertia changes due to increasing flattening as the body relaxes.

In this chapter the term $-\vec{\omega} \times (\mathbf{J} \cdot \vec{\omega})$ is activated by two model processes. First we simply deflect the rotation axis from its equilibrium position and then observe the induced free wobble. This non-physical process is studied in order to compare the numerical methods employed to solve the equation (1.4). Second studied process is more physical: the inertia tensor is modified by adding term $\mathbf{J}^{extra}$, which corresponds to adding some extra mass, e.g. on top of the surface of the body. The amount of extra mass is increased from zero to prescribed value within prescribed period of time. However, deformation due to e.g. surface loading is not computed - the value of $\mathbf{J}^{extra}$ is steadilly increased and then left constant[2].

3.1 Initial state

In order to separate the studied process from relaxation of the body, described in Chapter II, the body must be in rotational equilibrium when the process is started. Equilibrium is reached by setting $\vec{\omega}$ to a prescribed value and then

[1] however, the position of ω could have been chosen arbitrarily to get qualitatively same results, of course

[2] This simplification could easily be rid of be actually prescribing a certain surface load. However, the effect of induced deformation could complicate the results, which is not desired. The simplest possible process which involves extra mass located somewhere on the body is sought

evolving for the time needed for the body to relax. It makes no practical difference whether $\vec{\omega}$ is held constant or whether Liouville equation is solved simultaneously to decrease $|\vec{\omega}|$ as the body's flattening increases.

A noticable simplification is made throughout this chapter. Only model A is considered and self-gravity term $-\rho_0 \nabla \Phi$ is turned off in the equations of motion. This term is computed iteratively, with around 15 iterations needed when the term is computed from scratch in every time step. Omitting this term does not change the results qualitatively, it changes them only quantitavily and can thus be disregarded in this study. The simplifications allow for the results of this chapter to be easily reproduced within hours of computational time, yet do not bring any significant qualitative[3] change.

For the purpose of solving the Liouville equation the most important description of rotational relaxation is through the tidal Love number. The Love number approach is not adopted in the thesis, therefore Love numbers do not have to be computed. However, as described in equation (3.9) in Appendix B, the rotational deformation could be determined solely through convolution with the degree two tidal Love number, so certain attention to it is convenient. The tidal Love numbers are defined as ratios between the coefficients of spectral decomposition of gravitational potential induced by redistribution of mass due to deformation, i.e. Φ_{jm}, and coefficients of spectral decomposition of the disturbing potential that causes the deformation, i.e. φ_{jm} (e.g. Wu and Peltier, 1981). The definition assumes φ_{jm} to be multiple of the Dirac delta function in the time domain. Here we compute response to multiple of the Heaviside step function, i.e. φ_{20} is set to prescribed value at time $t = 0$ and then held constant (coefficient of degree two and order zero is chosen because that is the only non-zero coefficient when

[3]The effect of self-gravity is, however, rather significant on the degree two of the spectral decomposition. The importance of self-gravity decreases substantially as the characteristic spatial scale of density anomalies decreases (i.e. the degree of spectral decomposition coefficients increases). We work on the degree two, where the effect is the largest, increasing deformation approximately by a factor of 2

$\vec{\omega} = (0, 0, \omega_3)$). Figure 3.1 shows the evolution of $\frac{\Phi_{20}(t)}{\varphi_{20}(t)}$ for models A,B,C and for model A with self-gravity turned off, referenced as model D.

Figure 3.1: Evolution of $\frac{\Phi_{20}(t)}{\varphi_{20}(t)}$ for models A,B,C,D

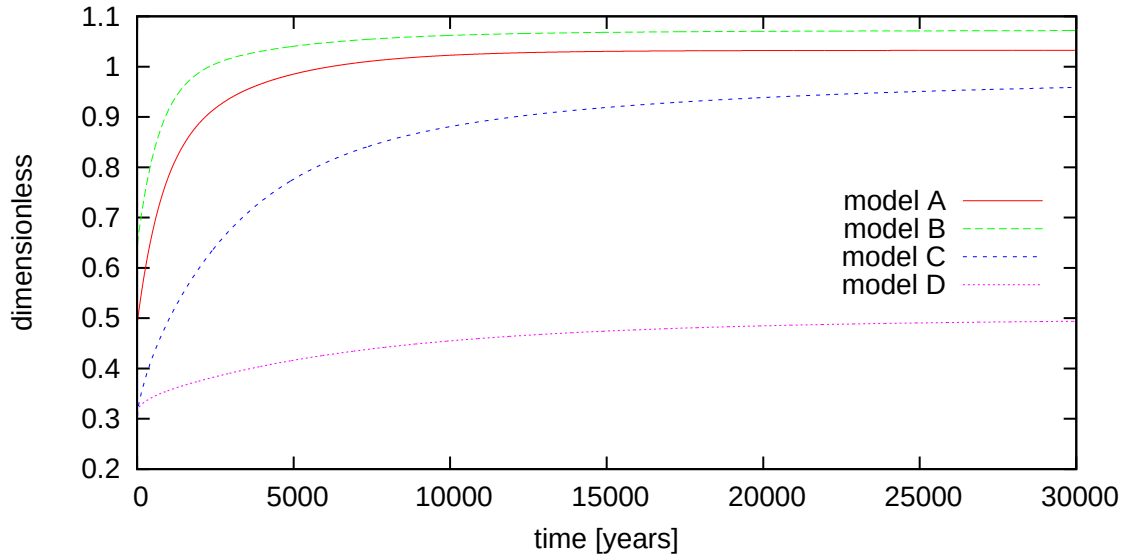

Important limits are the $t = 0$ limit and the $t \to \infty$ limit. The first one describs the instaneous, elastic response of the body, i.e. $k_{2,e}^T$, the latter describs the viscous (fluid) response, i.e. $k_{2,f}^T$. In the Appendix A it is shown that

$$\sigma_{Ch} := \frac{C - A}{A} \frac{k_f - k_2^T}{k_f} \Omega$$

defines the frequency of the free wobble in the linearized version of the Liouville equation. For model C, i.e. Earth-like model, the computed values are[4] $k_{2,e}^T = 0.28708$, $k_{2,f}^T = 0.97769$, $\sigma_{Ch} = 1.8205 \cdot 10^{-7}$. This value leads to free wobble period of 400 days, which differs from the observed value of around 433 days substantially. The discrepancy lies rather in incorrect value of $\frac{C-A}{A}$[5], than in incorrect value of $\frac{k_f - k_2^T}{k_f}$. Presumably, it could be explained be the existence of solid inner core, avoided in our study, or by the improper implementation of

[4]error estimates are not performed, the number of valid digits is chosen arbitrarily to 5

[5]The equilibrium value of $\frac{A}{C-A}$ is around 282 for model C, i.e. the Euler period is 282 days instead of 305 days which we get for the observed values of C and A.

density discontinuities within the mantle.

3.2 Numerical methods

The Liouville equations (1.4) can be written as:

$$-\mathbf{J}\cdot\frac{d\vec{\omega}}{dt}=\frac{d\mathbf{J}}{dt}\cdot\vec{\omega}+\vec{\omega}\times(\mathbf{J}\cdot\vec{\omega}), \tag{3.1}$$

which is a set of three non-linear, ordinary differential equations for the three components of $\vec{\omega}$. The time evolution of $\vec{\omega}$ is fully determined by $\mathbf{J}$, where $\mathbf{J}(t)$ depends on the entire time evolution of $\vec{\omega}(t)$, i.e. it is a functional[6]. In order to solve the set of ODEs (3.1), we need to be able to evaluate $\mathbf{J}$ for given $\vec{\omega}(t)$, which is done in the following manner: The memory terms at time t_n, i.e. components 4,5,6 of $\mathbf{y}$ in (2.6) hold information about the deformation of the body at time t_n. This deformation depends on the time evolution of $\vec{\omega}$ form time 0 to t_n. To get the value of $\mathbf{J}(\vec{\omega}(t))$, where $t > t_n$, $\vec{\omega}(t)$ is used to compute the force term $\rho_0\nabla\varphi$, i.e. the component 1 of $\mathbf{y}$, and the new values of memory terms are computed as $M_k(t) = M_k(t_n) + \frac{\mu(r)}{\eta(r)}(D^{k,2}_{jm}(r,t_n))(t-t_n)$. The self-gravity term $\rho_0\nabla\Phi$, which adds to components 1,2 of $\mathbf{y}$ is computed iteratively. Thus we gained $\mathbf{y}(t)$ and the set of equations (2.11) can be solved to get the desired value of $\mathbf{J}(t)$ from (2.12). The value of $\frac{d\mathbf{J}}{dt}$ is computed simply as $\frac{\mathbf{J}(t)-\mathbf{J}(t_n)}{t-t_n}$.

The above described procedure defines the coupling of the Liouville equation with the set of equations (2.6). The last step, necessary in order to employ standard numerical integrators, is to solve (3.1) for $\frac{d\vec{\omega}}{dt}$ when $-\mathbf{J}(t)$ and the right hand side of (3.1) are known (i.e. computed by the procedure described above). It is a linear problem with $\mathbf{J}$ being a 3×3 symmetric, positive definite matrix, solved by the Dsytrf, Dsytrs routines from the MKL library.

[6]Since $\mathbf{J}$ is symmetric positive definite tensor, the equations 3.1 could formally be written as $\frac{d\vec{\omega}}{dt} = -\mathbf{J}(\vec{\omega}(t))\cdot\left(\frac{d\mathbf{J}(\vec{\omega}(t))}{dt}\cdot\vec{\omega}+\vec{\omega}\times(\mathbf{J}(\vec{\omega}(t))\cdot\vec{\omega})\right) = f(\vec{\omega}(t))$. This is different from the traditional form of ODEs, $\frac{d\vec{\omega}}{dt} = f(\vec{\omega},t)$ because the right hand side in the latter case is a function of $\vec{\omega}$ and t, i.e. a function of four independet variables, not a functional. However, this difference is not an obstacle for numerical integrators of the set of ODEs, as explained below.

Several methods are tested to solve the equations (3.1). Three explicit: Euler method, fifth order Cash-Karp Runge-Kutta method, Bulirsch-Stoer method and two semi-implicit: Rosenbrock method and Bader-Deuflhard method. All the methods are described and subroutines provided in Numerical recipes for Fortran, Press et al. (1992). The Jacobian matrix, i.e. the partial derivatives of $f(y,t)$ in the formulation $\frac{dy}{dt} = f(y,t)$, that needs to be supplied when semi-implicit methods are implemented, is computed by numerical differencing.

The main obstacle to be encountered seems to be that once the term $\vec{\omega} \times (\mathbf{J} \cdot \vec{\omega})$ is activated, the rotation axis starts to wobble and the equations become stiff[7]. The typical problem of stiff set of equations is the following: "This is the generic disease of stiff equations: we are required to follow the variation in the solution on the shortest length scale to maintain stability of the integration, even though accuracy requirements allow a much larger stepsize." - Press et al. (1992). However, this is not our case. Our stepsize has to be a small fraction of the free wobble period, because $\vec{\omega}$ undergoes significant motion during the wobble and accuracy therefore demands the motion to be followed closely (i.e. accuracy requires to follow the shortest time scale in our case, not stability). The real problem is that high accuracy demands stepsize to be a fraction of the free wobble period, while the processes that induce polar motion which we wish to study take place on a completely different time scale - it is a problem of computational time.

To test the numerical methods and to demonstrate how accuracy is lost when stepsize is too large a non-physical process is selected. The body is rotated for time sufficient for it to reach equilibrium and then the rotation axis is suddenly deflected by a small angel, i.e. $\vec{\omega}$ is set to $\vec{\omega} = (0, \sin(\alpha)\omega_3, \cos(\alpha)\omega_3)$ where ω_3 is the equilibrium value. The evolution of ω_1 when simple Euler method is used with time step around $\frac{1}{300}$ of the free wobble period is shown in figure 3.2.

[7] "As soon as one deals with more than one first-order differential equation, the possibility of a stiff set of equations arises. Stiffness occurs in a problem where there are two or more very different scales of the independent variable on which the dependent variables are changing" - Press et al. (1992)

Figure 3.2: Divergence of $\omega_1(t)$ for large stepsize

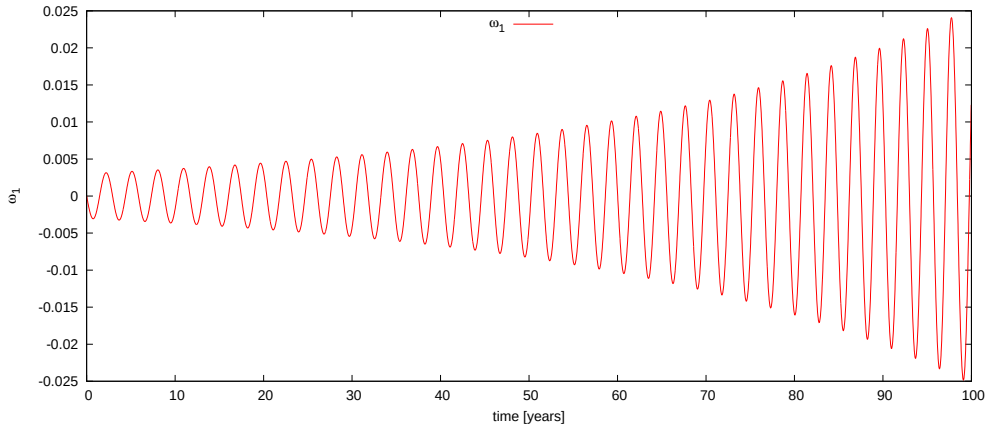

While the precission of the Euler method is determined by the size of the stepsize, the remaining methods have adaptative stepsize control. They make an estimate of the error for every attemted time step and allow the step only if the estimate is below prescribed value Δ_0[8]. Several choices of Δ_0 may be made. We set $\Delta_0(i) = \epsilon(|\omega(i)| + |h\frac{d\omega(i)}{dt}|)$, where h is the suggested stepsize and index $i = 1, 2, 3$ denotes components of the vector Δ_0. This choice leads to constant fractional errors except for when $\omega(i)$ crosses near zero (equation 16.2.8 in Press et al., 1992)[9]. For sufficiently small value of ϵ high precission solutions are obtained and thus all the methods yield the same result. Figure 3.3 shows evolution of ω_1 when computed by all the tested methods with $\epsilon = 10^{-10}$, the curves are identical.

For computational reasons we divided the equation 3.1 by two scaling factors to work with normalized $\bar{\vec{\omega}} = (m_1, m_2, m_3) := \frac{\vec{\omega}}{\Omega_0}$ and $\bar{\mathbf{J}}$, where Ω_0 is defined as $|\vec{\omega}|$ in the equilibrium. In the figures below m_i is used instead of ω_i to describe the rotation vector, m_3 has different meaning than in the notation introduced in Appendix A.

For the test depicted in 3.3, stepsize of the Euler method was chosen approximately 3×10^{-7} of the free wobble period to have extremly high accuracy for referential purposes[10]. Though all the methods yield the same results, the compu-

[8] If not, the suggested time step is shortened. If the error estimate is much smaller than Δ_0 the next suggested time step is prolonged.

[9] Since accumulation of error is a problem in tracing the wobble, the choice $\Delta_0(i) = \epsilon|h\frac{d\omega(i)}{dt}|$ should also be thoroughly tested. It is not done in the thesis

[10] The time needed to evolve 100 years was 22500 seconds

Figure 3.3: $m_1(t)$ computed by different methods with high precission

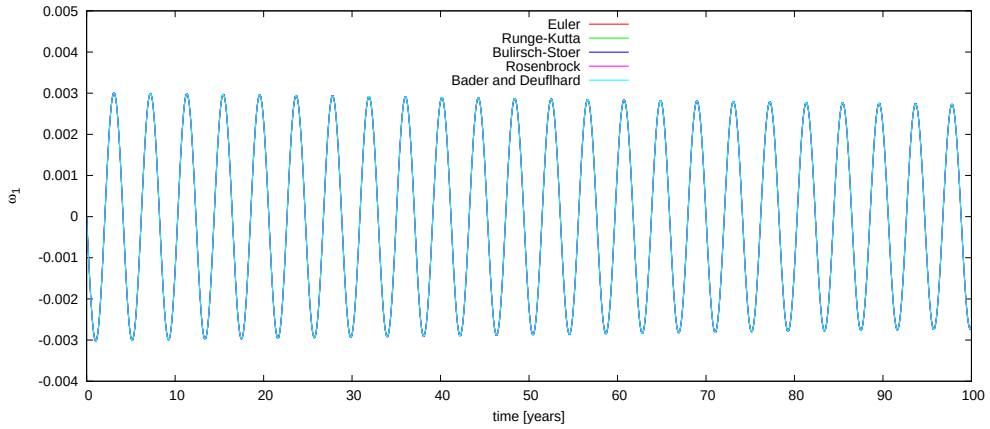

tational time needed to reach them varies substantially. To ilustrate the different behavior of the methods, computational times for $\epsilon = 10^{-10}$ and $t_{final} = 100$ years are shown in table 3.1.

Table 3.1: Computational time for a test case

Method	Computational time
Runge-Kutta	753 s
Bulirsch-Stoer	21303 s
Rosenbrock	12140 s
Bader and Deuflhard	976 s

The comparison of the methods based on computational times needed for given ϵ and t_{final} is not complete, because the error estimates computed by the methods themselves are general estimates, regardless of the problem at hand. Therefore, for a given problem, especially for atypical one in which the error tends to accumulate in one direction (it pushes the rotation axis away from the center of the wobble, as shown in figure 3.2), the actual error accumulated by different methods may vary, even though ϵ is set the same. For this reason, detail analysis of accuracy is necessary. However, it is left for further development. The reason why the methods strongly vary in the demanded computational time is of rather technical background, related to how exactly the Liouville equations are coupled with the equations of motion. The fact that semi-implicit methods do not dominate over embedded Runge-Kutta method is also left unexamined.

3.3 Artificial loading

Following process is studied in the final section: artificial increment $\mathbf{J}^{extra}(t)$ is added to $\mathbf{J}$(t), $\mathbf{J}^{extra}(t)$ linearly increasing from time t_{start} to time t_{end} and then held constant. The components of $\mathbf{J}^{extra}(t_{end})$ are chosen to be:

$$\mathbf{J}^{extra} = \begin{pmatrix} \cos^2(\frac{\pi}{4}) & 0 & -\sin^2(\frac{\pi}{4}) \\ 0 & 1 & 0 \\ -\sin^2(\frac{\pi}{4}) & 0 & \sin^2(\frac{\pi}{4}) \end{pmatrix} r_0^2 M_E, \tag{3.2}$$

which corresponds to mass M_E located at $(r_0, \frac{\pi}{4}, 0)$. It can be seen directly from the definition of $\mathbf{J}$ for $\rho = M_E\delta(r_0, \frac{\pi}{4}, 0)$. This extra mass is not incorporated into the equations of motion (2.1), which means that it causes no deformation of the body. For example, if the extra mass was on surface of the body, no isostatic compensation would occur.

This artificial process is designed to test the developed tool in two key aspects. Its purpose is to explore the method's ability to predict polar wander for long-term phenomena (e.g. millions of years) and to reconstruct the results obtained by previous authors using methods described in Appendices A and B.

To compare the results with equation (3.7) from Appendix A, it is important to realize that its derivation followed directly from averaging the solution of (3.5)[11], which means that variations in the inertia tensor arising from instaneous elastic rotational deformation, given by equation (3.8), need to be included when the excitation function Ψ is evaluated. In the presented case, the equation (3.6) thus becomes:

$$\psi_1 = \frac{1}{(C-A)}(j_{13}^R + j_{13}^{extra}) = \frac{1}{(C-A)} j_{13}^{extra} + \frac{k_2^T}{k_f} m_1.$$

After substituting into (3.7) we get the final form of the linearized equation, to

[11] In fact, Martinec and Hagedoorn (2005) averaged the solution over the Euler period - $\frac{2\pi}{\sigma_r}$ - which is not the true period of the free wobble for the Earth. The reason for this slight inconsistency is closely related to the fact argumented below: variations in the inertia tensor arising from instaneous elastic rotational deformation, given by equation (3.8), are not extracted from excitation function Ψ before averaging

be compared with the results gained by the method developed in this thesis:

$$\left(1 - \frac{k_{2,e}^T}{k_{2,f}^T}\right) \bar{\mathbf{m}}_1(t) = \frac{1}{(C-A)} j_{13}^{extra}(t) \tag{3.3}$$

In other words, the equation $\bar{\mathbf{m}}(t) = \bar{\Psi}(t)$ modifies to $\left(1 - \frac{k_{2,e}^T}{k_{2,f}^T}\right) \bar{\mathbf{m}}(t) = \tilde{\Psi}(t)$, where $\tilde{\Psi}(t)$ is excitation function from which elastic rotational deformation is extracted - in our case it is determined fully by the knowledge of $\mathbf{J}^{extra}$.

Figure 3.4 shows evolution of $m_1(t)$ computed from equation (3.3) and $m_1(t)$ computed by our method[12]. Mass M_E was set equal to 10^{10} kg, r_0 was set equal to r^{surf}. The process started at time $t_{start} = 10$ years and the increasing of extra mass was stopped at $t_{end} = 100$ years.

Figure 3.4: 150 year evolution of $m_1(t)$ for artificial loading process

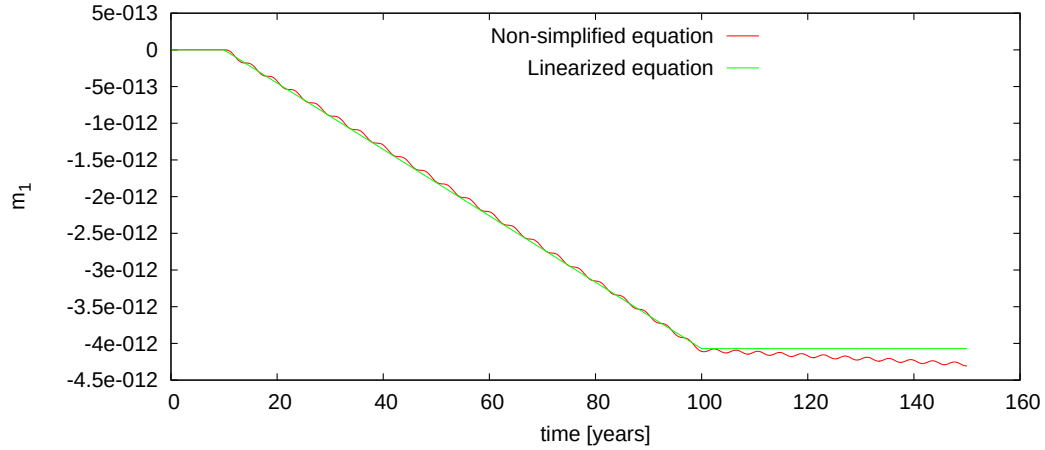

Several phenomena may be observed in figure 3.4. Small wobble is exited, maintaining constant amplitude. In fact, though not mentioned in the respective commentary, figure 3.3 shows small damping of the wobble. The ability to show excitation and damping of the free wobble is one of the main advantages of the method developed in the thesis and should be thoroughly analyzed in future work.

The comparison with solution of the linearized Liouville equation seems to have passed the test. The most obvious discrepancy between the two solutions is after the time t_{end}: while the linearized equation gives constant $m_1(t)$ once

[12]Namely Runge-Kutta with $\epsilon = 10^{-7}$ - for this process the values of ϵ need to be set differently from the process studied in previous section

$j_{13}^{extra}(t)$ becomes constant, the $m_1(t)$ resulting from our code continues to evolve towards lower values. The explanation lies in the fact that the linearized version of the Liouville equation does not allow for the readjustment of the long-term equatorial bulge to take place.

On the other hand, in the second method described in Appendix B, developed by Ricard et al. (1993), the readjustment of long-term equatorial bulge is the key factor in determining the polar wander. The solution of their equation (3.10) is not reproduced in the thesis, so only qualitative aspects of the solutions can be compared. Common feature of the results presented by Ricard et al. (1993) is that the rotation axis moves towards a negative geoid anomaly to end up in the center of it eventually. We try to reconstruct this aspect of the solution.

The studied effect can briefly be explained as follows: the extra mass[13] shifts the main axis of inertia away from the equilibrium position, in the direction away from the extra mass. This causes the rotation axis to wobble around the new position, and after some time the long-term equatorial bulge readjusts itself, shifting the main axis of inertia further away from the extra mass. This process continues untill the extra mass is located on the equator, i.e. as far from the rotation axis as possible, maximizing its contribution to the largest moment of inertia. The time needed for the long-term equatorial bulge to readjust plays crucial role in determining the time it takes for the extra mass to move to the equator.

Figure 3.5 shows longtime evolution of m_1 and m_3. Clearly, the effect described above has taken place, since the final position of the rotation vector is as expected - the extra mass lies on the equator. Parameters of the process, i.e. M_E, r_0, t_{start}, t_{end} were set equal to: $M_E = 10^{19}$ kg, $r_0 = r^{surf}$, $t_{start} = 10$ years, $t_{end} = 100$ years. Large value of M_E explains why the time needed for the rotational axis to settle is much shorter than observed in Ricard et al. (1993) for

[13]i.e. positive geoid anomaly. If dynamic topography is taken into consideration, crucial is whether its contribution to geoid is stronger or weaker than the contribution of the mass itself.

sinking slabs. In future work, the results should be compared with the curves depicted in Ricard et al. (1993). In order to do so, appropriate value of M_E, i.e. M_E that gives the same geoid anomaly as the studied sinking slab, and comparable body model must be chosen.

Figure 3.5: Long-term evolution of $m_1(t)$,$m_3(t)$ for artificial loading process

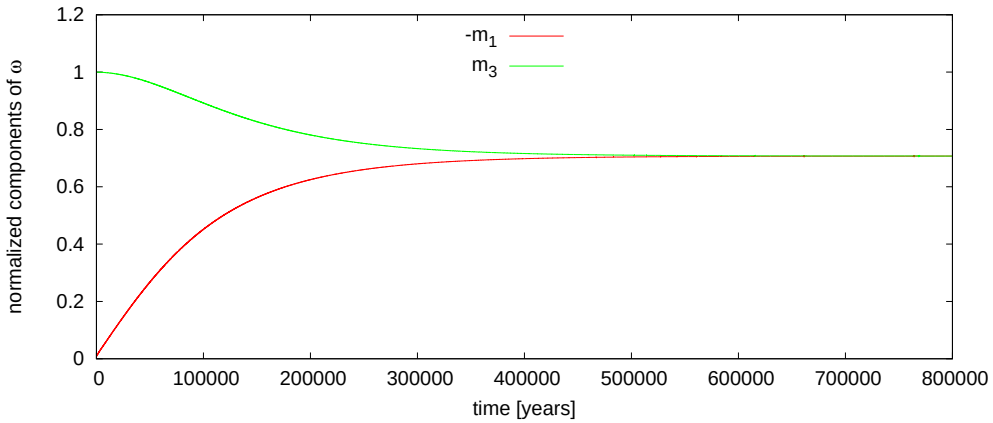

Since only simplified model was used to compute the polar wander, important question that immidiately arises is whether the method could be applied to predict the long-term polar wander for complex models. The time needed to compute the results depicted in figure 3.4 was around 8000 seconds on a 3.2GHz processor. For the same model, only with the self-gravity term not excluded from the equation of motion, the necessary computational time would be multiplied by the number of iterations needed to compute the self-gravity term, which is around 10. That means that for simple models the method is capable of computing the polar wander even for millions of years. However, the cost to involve self-gravity into the equations is quite high. It would be convenient to replace the iterative procedure by implementing self-gravity through changing the components of $\mathbb{A}$ in (2.11). Some of the properties of $\mathbb{A}$ would be destroyed, but the computational time would still probably decrease substantially.

The artifical loading process was computed also for model C with 10 iterations used to compute the self-gravity term. It takes around 4000 s to evolve 10000 years. This gives computational time around 100 hours to evolve a million years, i.e. the method can be used for long term prediction of polar wander even for

complex models, though it is on the edge of computational capability. Detail analysis of accuracy of the obtained solutions is left for future development, as well as analysis of the changes of the free wobble amplitude.

Conclusion

Theoretical background of the Liouville equation is analyzed in the first part of the thesis. It provides alternative derivation of the equation, with approach based on evaluating the effect of fictious forces in the law of balance of angular momentum, when formulated in a non-inertial frame of reference. It explains how Coriolis, Euler and centrifugal forces are related to the terms in the Liouville equation. Also, the relation between the relative angular momentum and acting forces in the equation of motion is explained.

Two topics are further examined in the thesis. Computation of rotational deformation of a viscoelastic body is the first one of them. It is studied in Chapter II. Eulerian approach is used to formulate the set of governing field equations, geometrical linearization and other traditional geophysical approximations are employed. The equations are solved directly in the time domain and the studied body is assumed to have incompressible, viscoelastic mantle and fluid core. Deformation of inhomogeneous models with radially dependent density, viscosity and shear modulus is computed.

The studied process in Chapter II is reaching of the rotational equilibrium, i.e. reaching the state in which the body rotates with constant angular velocity and deviatoric part of the stress tensor is zero. This state is reached for three chosen models: a homogeneous body, body with simple density profile and an Earth-like model. The equilibrium is used as initial state for processes studied in the third chapter. Before that, the developed code is checked using isostatic compensation test, in which the body is subjected to surface loading. The response in the $t \to \infty$ is such as to compensate the load by the induced topography, deviatoric part of the stress tensor being again zero.

The key topic of the thesis is finding numerical solution of the non-linear Liouville equations. The equations are solved in the time domain, where they can easily be coupled with equations for rotational deformation. Basic numerical

methods are tested. It is shown that even the fifth order embedded Runga-Kutta integrator (i.e. often the first choice for integrating ODEs) is capable of computing polar wander for homogeneous model for millions of years. Long-term polar wander prediction for complex models also seems to be possible within weeks of computation, but was not performed in the thesis because of the time necessary to do so.

A specific non-physical process is chosen to compare the solution of the non-simplified Liouville equation with solutions reached by approximative methods developed by previous authors. Comparison with solution of the linearized Liouville equation is conducted quantitatively. The solutions coincide on average. Comparison with the method developed by Ricard et al. (1993) is carried out only qualitatively, both solutions show the same features on average.

Two tasks seem important in order to complete the present work. First is detail analysis of accuracy of the solutions gained by the implemented numerical methods. At this moment, it is not clear what is the computational time needed for a specified physical process for a chosen model of the planet-sized body. Second task is thorough comparison with the approximative methods, performed for various processes. This would allow us to see where actually lie the applicational limits of the approximative methods. Answer to both these questiones is only outlined in the thesis. However, the results seem promising.

The main disadvatage of the developed method are high computational demands for complex models. The approximative methods dominate in this respect when solving problems which fall within their applicational limits. On the other hand, the developed tool has two advantages. First is that no specific conditions are required for the solution to be valid, since no approximation is made in formulating the Liouville equation. Second is that the solution contains phenomenom which is filtered out by the approximative methods - the free wobble of the rotational axis. Excitation and damping of the amplitude of the free wobble can thus be measured when analyzing the numerical solution.

Appendix A - The linearized Liouville equations

Munk and MacDonald (1960) proposed the following perturbation scheme (notation used in the following equations is slightly modified from the one used in Munk and MacDonald):

$$\begin{array}{ccc} J_{11} = A + j_{11} & J_{22} = A + j_{22} & J_{33} = C + j_{33} \\ J_{12} = j_{12} & J_{13} = j_{13} & J_{23} = j_{23} \\ \omega_1 = \Omega m_1 & \omega_2 = \Omega m_2 & \omega_3 = \Omega(1 + m_3) \end{array}$$

If we neglect the products and squares of $\frac{j_{ij}}{C}, m_i, \frac{h_i}{\Omega C}$, as they are small dimensionless numbers (for the case of the Earth), the Liouville equations decouple into two:

$$i\frac{\dot{\mathbf{m}}}{\sigma_r} + \mathbf{m} = \Phi, \quad \dot{m}_3 = \dot{\phi}_3. \tag{3.4}$$

The first one is called the polar motion (PM) equation, the second length of day (LOD) equation, for that is what they govern. Complex notation was introduced: $\mathbf{m} = m_1 + im_2, \quad \Phi = \phi_1 + i\phi_2$, and the excitation functions ϕ_1, ϕ_2, ϕ_3 have the following definition:

$$\begin{array}{c} \Omega^2(C - A)\phi_1 = \Omega^2 j_{13} + \Omega\dot{j}_{23} + \Omega h_1 + \dot{h}_2 - L_2 \\ \Omega^2(C - A)\phi_2 = \Omega^2 j_{23} + \Omega\dot{j}_{13} + \Omega h_2 + \dot{h}_1 - L_1 \\ \Omega^2 C\phi_3 = -\Omega^2 j_{33} - \Omega h_3 - \Omega \int_0^t L_3 dt \end{array}$$

The excitation function has to be computed for the studied process (e.g. loading, winds) in order to determine its effect on polar wander. The equation 3.4 can also be written in the form:

$$i\frac{\dot{\mathbf{m}}}{\sigma_r} + \mathbf{m} = \Psi - \frac{i}{\Omega}\dot{\Psi} + \frac{L}{(C - A)\Omega^2}, \tag{3.5}$$

where angular excitation function $\Psi = \psi_1 + i\psi_2$ is defined

$$\psi_1 = \frac{1}{(C-A)\Omega}(\Omega j_{13} + h_1), \quad \psi_2 = \frac{1}{(C-A)\Omega}(\Omega j_{23} + h_2) \tag{3.6}$$

and complex notation $L = L_1 + iL_2$ was introduced (e.g. Martinec and Hagedoorn, 2005).

Martinec and Hagedoorn (2005) showed by direct averaging of the solution of the equation that for the case of GIA (glacial isostatic adjustment) the equation can be written (no external torque assumed, $\vec{h}(t)$ set to zero):

$$\bar{\mathbf{m}}(t) = \bar{\Psi}(t), \tag{3.7}$$

where barred quantities denote the average over $\frac{2\pi}{\sigma_r}$. Analogous step - neglecting the time derivatives in $i\frac{\dot{\mathbf{m}}}{\sigma_{Ch}} + \mathbf{m} = \Psi - \frac{i}{\Omega}\dot{\Psi} + \frac{L}{(C-A)\Omega^2}$ was done by Wu and Peltier (1984) while solving the equation in the Laplace domain.

In the scheme above, long-term rotational deformation (the equatorial bulge) was already accounted for, as C, A, A are used in 3.3 (C, A, A being the principal moments of inertia for zero m_1, m_2, m_3). The instaneous elastic response to centrifugal potential that causes instaneous, slight readjustment of the equatorial bulge, can be expressed (again neglecting the squares and products of m_i):

$$\begin{aligned} j_{11}^R = j_{22}^R = -\tfrac{2k_2^T}{3k_f}(C-A)m_3, \quad & j_{33}^R = \tfrac{4k_2^T}{3k_f}(C-A)m_3 \\ j_{13}^R = \tfrac{k_2^T}{k_f}(C-A)m_1, \quad & j_{23}^R = \tfrac{k_2^T}{k_f}(C-A)m_2 \end{aligned} \tag{3.8}$$

When computing the period of the free wobble, excitation function due to solely the elastic rotational deformation is considered, and equation the PM equation (3.4) becomes:

$$i\dot{\mathbf{m}} + \sigma_{Ch}\mathbf{m} = \Phi,$$

where the Chandler frequency σ_{Ch} has simple relation to the Euler frequency σ_r:

$$\sigma_r := \frac{C-A}{A}\Omega, \quad \sigma_{Ch} := \sigma_r \frac{k_f - k_2^T}{k_f}$$

.

Appendix B - The quasi-fluid approximation

The above described perturbation scheme is convenient only "as long as the poles of figure and rotation do not wander too far from the reference pole" [14]. Also, since only the elastic response to motion of the rotation pole was considered, the linearized equation is not capable of accounting for the readjustment of the long-term equatorial bulge. A more general method, which accounts for this readjustment, was developed by Ricard et al., 1993. For the case of no external torque, they proceed as follows. First, Tisserand's axes are chosen:

$$\frac{d}{dt}\left(\mathbf{J}\cdot\vec{\omega}\right)+\vec{\omega}\times\left(\mathbf{J}\cdot\vec{\omega}\right)=0$$

Next, the inertia tensor is evaluated with the use of the viscoelastic tidal Love numbers. The driving process is surface loading, described by $C_{ij}(t)$ (the method is designed to study the post glacial rebound):

$$J_{ij}(t)=\mathbf{I}\delta_{ij}+\frac{k_2^T(t)a^5}{3G}*[\omega_i(t)\omega_j(t)-\frac{1}{3}\omega^2(t)\delta_{ij}]+[\delta(t)+k_2^L(t)]*C_{ij}(t) \quad (3.9)$$

a being the radius of the Earth, δ_{ij} the Kronecker symbol, G the gravity constant and $*$ denoting the time convolution. The viscoelastic Love numbers used in this expression are traditionally computed in the Laplace domain, using the normal modes technique proposed by Peltier (1974). They can generally be written as follows:

$$k(s)=k_e+\sum_{i=1}^{M}\frac{k_i}{s-s_i},$$

where M is the number of relaxation modes, $\frac{-1}{s_i}$ their relaxation times and k_i their amplitudes. The main trick involves realizing that for sufficiently slow process

[14] Munk and MacDonald, 1960

most of the tidal and loading relaxation modes get fully relaxed within a time-step on which the excitation function changes. For the tidal and loading viscoelastic Love numbers the authors, under these conditions, get (s denoting the Laplace transform variable):

$$k^T(s) = k_f^T(-T_1 s), \quad k^L(t) = k_f^L + \frac{k_{M1}^L}{s_{M1}} e^{s_{M1} t}$$

where $T = \frac{1}{k_f^T} \sum_{i=1}^{M} \frac{k_i^T}{s_i^2}$, k_f denotes the fluid limit ($t \to \infty$, i.e., $s = 0$) and M1 stands for the relaxation mode caused by the 670km depth chemical discontinuity. After substitution of these expressions into (3.9) and after neglecting the terms in $\ddot{\omega}$ and $\dot{\omega}^2$ - important step, though not discussed in Ricard et al., 1993 (a possible explanation of this step can be found in Lefftz et al., 1991), we finally get:

$$A_{ij}(\vec{\omega})\dot{\omega}_j + B_{ij}(\vec{\omega}, E, \dot{E})\omega_j = 0 \tag{3.10}$$

where

$$A = \frac{k_f^T T_1 a^5}{3G} \begin{pmatrix} \frac{3GI}{k_f^T T_1 a^5} & \omega^2\omega_3 & -\omega^2\omega_2 \\ -\omega^2\omega_3 & \frac{3GI}{k_f^T T_1 a^5} & \omega^2\omega_1 \\ \omega^2\omega_2 & -\omega^2\omega_1 & \frac{3GI}{k_f^T T_1 a^5} \end{pmatrix} \quad B = \begin{pmatrix} \dot{E}_{11} & \Sigma_3 & -\Sigma_2 \\ -\Sigma_3 & \dot{E}_{22} & \Sigma_1 \\ \Sigma_2 & -\Sigma_1 & \dot{E}_{33} \end{pmatrix}$$

$\Sigma_k := E_{ki}\omega_i$, $E_{ij}(t)$ is obtained by convolving $C_{ij}(t)$ with $\delta(t) + k^L(t)$. "As the diagonal terms of A are smaller than the non-diagonal terms, a further approximation could be to neglect them (Lefftz 1991)" [15]. Neglecting the diagonal terms of A is equivalent to solving $\mathbf{J}\cdot\vec{\omega} = \alpha\vec{\omega}$, i.e. equation equivalent to the one derived at the end of section 1.3: $-\vec{\omega} \times (\mathbf{J} \cdot \vec{\omega}) = 0$

[15] Ricard et al., 1993

Bibliography

[1] Dziewonski A. M., Anderson D. L., 1981: *Preliminary reference Earth model*, Physics of the Earth and Planetary Interiors, **25** (1981), 297-356.

[2] Golle O., Dumoulin C., Choblet G., Čadek O., 2012: *Topography and geoid induced by a convecting mantle beneath an elastic litosphere*, Geophys. J. Int., **189** (2012), 55-72.

[3] Gerya T. V., Yuen D. A., 2003: *Characteristics-based marker-in-cell method with conservative finite-differences schemes for modeling geological flows with strongly variable transport properties*, Phys. Earth. Planet. Inter., (2003) **140**(4), 293-318.

[4] Hanyk L., Yuen D., Matyska R., 1996: *Initial-value and modal approaches for transient viscoelastic responses with complex viscosity profiles*, Geophys. J. Int., (1996) **127**, 348-362.

[5] Havránek A., 2002: *Klasická mechanika I.*, Univerzita Karlova v Praze, Karolinum, 2002.

[6] Jones M. N., 1985: *Spherical Harmonics and Tensors for Classical Field Theory*, Research Studies Press, Letchworth, England (1985).

[7] Lefftz M., Legros H., Hinderer J., 1991: *Non-linear equations for the rotation of a viscoelastic planet taking into account the influence of a liquid core*, Celestial Mech. and Dynamical Astr., (1991) **52**, 13-43.

[8] Legros H., Lefftz M., 1993: *On the fluid and viscoelastic deformation of the planets*, Celestial Mech. and Dynamical Astr., (1993) **57**, 247-278.

[9] Martinec Z., Hagedoorn J., 2005: *Time-domain approach to linearized rotational response of a three-dimensional viscoelastic earth model induced by glacial-isostatic adjustment: I. Inertia-tensor perturbations*, Geophys. J. Int., **163** (2005) 443-462.

[10] Martinec Z., 2003: Continuum Mechanics - Lecture Notes, Department of Geophysics, Charles University in Prague, (2003)

[11] Matas J., 1995: *Diploma thesis: Mantle viscosity and density structure*, Charles University in Prague, Department of Geophysics, 1995.

[12] Munk W., MacDonald G. J. F.: *The Rotation of the Earth: A Geophysical Discussion*, Cambridge University Press, 1960.

[13] Novotný O., 1998: *Motions, Gravity Field and Figure of the Earth*, Universidade Federal da Bahia, Salvador, 1998.

[14] Peltier W. R., 1974: *The impulse response of a Maxwell Earth* Rev. Geophys. Space Phys., **12** (1974), 649.

[15] Press H. W.,Teukolsky S. A., Vetterling W. T., Flannery B. P., 1992: *Numerical Recipes in Fortran 77: The Art of Scientific Computing*, Cambridge University Press, 1992.

[16] Ricard Y., Spada G., Sabadini R., 1993: *Polar wandering of a dynamic earth*, Geophys. J. Int. **113** (1993), 284-298.

[17] Richards M. A., Ricard Y., Lithgow-Bertelloni C., Spada G., Sabadini R., 1997: *An Explanation for Earth's Long-Term Rotational Stability*, Science, **275** (1997) 372-375.

[18] Spada G., Sabadini R., Ricard Y.: *On a particular solution of the nonlinear Liouville equation*, Geophys. J. Int., **114** (1993) 399-404.

[19] Tobie G., Čadek O., Sotin C., 2008: *Solid tidal friction above a liquid water reservoir as the origin of the south pole hotspot on Enceladus*, Icarus, **196** (2008) 642-652.

[20] Varshalovich D. A., Moskalev A. N., 1988: *Quantum Theory of Angular Momentum*, World Scientific Publishing Company, Incorporated, 1988.

[21] Wu P., Peltier W. R., 1982: *Viscous gravitational relaxation*, Geophys. J. R. astr. Soc. **70**(1982), 435-438.